DESIGN AND SIMULATION OF FILM BULK ACOUSTIC RESONATOR

A Dissertation submitted in fulfillment of the requirements for the Degree

of

MASTER OF ENGINEERING

in

Electronic Instrumentation & Control Engineering

Submitted by

Yatin Kumar
Regd. No. 801351030

Under the Guidance of

Dr. Kamaljit Rangra
Chief Scientist
SNTG Department
CSIR-CEERI, Pilani

Dr. Ravinder Agarwal
Professor and Head
EIED
Thapar University

July 2015

Electrical and Instrumentation Engineering Department

Thapar University, Patiala

(Declared as Deemed-to-be-University u/s 3 of the UGC Act., 1956)

Post Bag No. 32, Patiala – 147004

Punjab (India)

Central Electronics Engineering Research Institute
(Council of Scientific & Industrial Research)
Pilani – 333 301 (Rajasthan) India.

CERTIFICATE

I hereby certify that the work which is presented in the Project entitled "Design and simulation of film bulk acoustic resonator" is submitted by **Yatin Kumar (ID-801351030)** in partial fulfillment of the requirement for the award of the degree of **Master of Engineering** in Electronics Instrumentation and Control Engineering embodies the work carried out by him under my supervision and guidance at SEM group, Sensor and Nano-Technology Group Division, Central Electronics Engineering Research Institute **[CEERI]**, Pilani (Rajasthan) w.e.f. January 2015 – June 2015. The work submitted has in my opinion reached a level required for being accepted for examination. The results embodied in this Dissertation Project work to the best of my knowledge have not been submitted to any other University or Institute for award of any degree or diploma.

Signature of Training In-Charge

Date:

Place: Pilani

Signature of the Guide

Dr. Kamaljit Rangra
(Chief Scientist)

DECLARATION

I hereby certify that the work which is presented in dissertation entitled, "Design and Simulation of Film Bulk Acoustic Resonator", in partial fulfilment of the requirements for the award of the degree of Master of Engineering in Electronic Instrumentation and Control, submitted to Electrical & Instrumentation Engineering Department of Thapar University, Patiala is as authentic record of my own work carried under the supervision of Dr.Ravinder Agarwal. It refers others researcher's work which are duly listed in the reference section. The matter contained in this dissertation has not been submitted neither in part nor in full to any other degree to any other university or institute except as reported in text and references.

Place: Patiala
Date: 13/07/2015

Yatin Kumar
Roll No.: 801351030

It is certified that the above statement made by the student is correct to the best of my knowledge and belief.

Date: 13/07/2015

Dr. Ravinder Agarwal
Professor
Electrical & Instrumentation Engineering Department
Thapar University, Patiala

Countersigned by:

Head
Electrical & Instrumentation Engineering Department
Thapar University, Patiala

Dean (Academic Affairs)
Thapar University, Patiala

ACKNOWLEDGEMENT

There is always a sense of gratitude which one expresses to others for helpful service they render during all phases of life. I too, would like to thank all those who helped me directly and indirectly in completion of this work. It was a matter of privilege and prestige to undergo training in an esteemed organization such as CSIR-CEERI, PILANI.

First of all, I would like to thank **Dr.Ravinder Agarwal**, with whose guidance and constant effort I got opportunity to work in research field in such a great professional environment of CEERI. I would like to thank him for his constant motivation and support throughout the project.

I am grateful to **Dr.Chandrashekhar**, Director of Central Electronics Engineering Research Institute, Pilani, without whom I would never have had an opportunity to work at CEERI, Pilani.

It is my proud privilege and pleasure to work under the ablest supervision of **Dr.KamaljitRangra**, Chief Scientist, Sensor and Nanotechnology Group, CSIR-CEERI, Pilani. I am feeling honoured in bestowing upon him my overwhelming sense of gratitude, unfathomable feeling of regards and heartfelt indebtedness to my most honourable supervisor.

I would also express my sincere gratitude towards **Mr. Deepak Bansal**, **Mr. Prem Kumar**, **Mr. AnuroopBajpai, Mr. Surender Gaur** and all other members of SEM Lab for their expert guidance which made this work possible.

I would like to express my sincere gratitude and sincere thanks to my Parent and Family for their strong support in all situations.

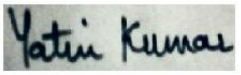

Yatin Kumar

Table of Contents

List of Figures

List of Tables

Abstract

Number of applications have emerged using FBAR like mass detector, gas sensor, humidity sensor, UV sensor, DNA and protein detector and many more, which motivates the researchers to work further to make most of it. Design and simulation of FBAR is done for the variation in number of parameter and there effects on FBAR. The bulk etching design is selected for the simulation and the 5 different combinations of electrodes are simulated for the parameters like quality factor, coupling coefficient, resonant frequency, impedance response and figure of merit (FOM). In this thesis the analytical results are identified for the same configuration of the electrodes by using the one dimension (Z-axis) analytical approach by using the simple piezoelectric derivations.

The losses across the FBAR are identified. Also, methods of suppressing the spurious modes are discussed and simulated. The simulation is carried out for the anchor losses effect on the quality factor and resonant frequency. The effect of damping factor variation is simulated and shown the inverse relationship in between them. The methods for suppression of spurious modes are simulated in the Comsol as well as CoventorWare. The results suggest an effective suppression. The effect of change in the area is simulated to identify the effect on the impedance which helps to connect the filter in the communication line with the maximum power transfer condition satisfied.

Centre mass loading technique is simulated and the sensitivity is measure for the mass change. This technique is used in many applications like detection of the RDX particles in the environment. Also, the simulation is carried out in Comsol software to find the change in sensitivity for the shifting of mass from centre position to the corner position. The sensitivity comes out to be decreased as the mass shifted towards the corner.

Butterworth Van-Dyke equivalent circuit parameters are also used to find out the resonant frequency obtained from the simulation by using the different equations.

AlN is used as the choice for the piezoelectric material because of its superior acoustic properties from the other materials. Different types of electrodes are used viz. Aluminium, Platinum, Tungsten, Molybdenum and combination of electrodes.

AlN layer is deposited by the sputtering technique over the Aluminium layer. Silicon is taken as the substrate over which the cleaning and photolithography is done to form the different patterns expose. Sputtered AlN layer is characterised by using FTIR, SEM, and EDS *etc*.

Chapter 1 Introduction

Full bulk acoustic wave resonator (FBAR) is used mostly in the communication due to the reduced size and reduced power consumption. Many features and its commercial success caught the attention of researcher.

1.1 FBAR basics

Thin film bulk acoustic wave resonator is the device having a piezoelectric layer sandwiched between two electrodes and acoustically isolated (means the acoustic energy generated in the system remains in the system). This device has the tendency to pass the only frequencies which are matching to its acoustic resonant frequency and reject all other (except harmonics). This filter has very steep bandwidth. This structure also behaves like a capacitor, generator, motor *etc*.

At electrode a voltage V is applied to induce the electric field (E) and then electric density displacement (D) in polling axis of structure. It causes the mechanical deformation in the axis of E and then strain in all three directions. The speed of mechanical deformation depends on the crystal orientation. Now, due to applied voltage on one electrode, structure starts deforming and starts to propagate into the bulk of the material (because the time varying effect) according to the frequency of the signal. Electrical signal generates the mechanical resonance in the structure and this mechanical resonance is turned into the electrical domain for the output by other electrode (simple working of the piezoelectric material i.e. direct and inverse effect).

There are three possible modes of propagation of the wave namely longitudinal, transverse and surface waves (combination of both). Also, there are plate waves along the parallel plates and these waves affect the performance of the FBAR by inserting the parasitic effects.

Let thickness is 2d and sandwiched between 2 electrodes, material has acoustic velocity v, and then the mechanical resonance condition of the system is simply

$$\omega_n = (n+1)\frac{\pi}{2}\frac{v}{d}$$, where n=0, 1, 2..... (Harmonics)

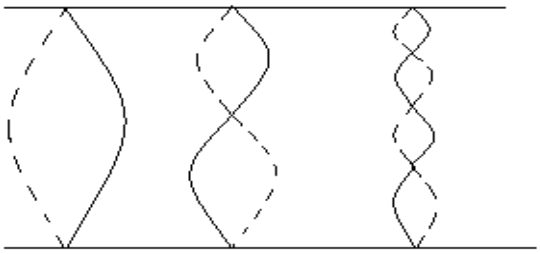

n=0 n=1 n=2

Figure 1-1 Wave propagation in material

If first harmonic is i.e. n = 0, then resonant frequency which will pass is

$$\frac{\pi v}{2d} = \omega_n$$

$$\frac{\pi v}{2d} = \pi f$$

$$f = \frac{v}{2d}$$

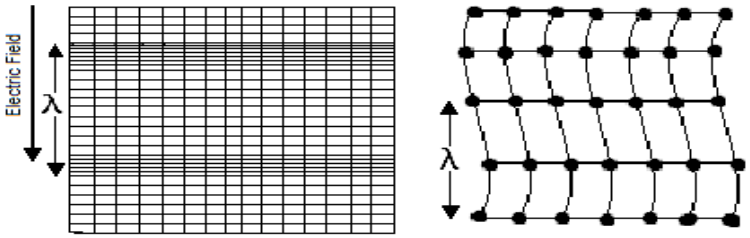

Figure 1-2 Longitudinal and transverse wave propagation

Figure 1-2 shows the piezoelectric crystal atomic structure deformation due to time varying electric field. The fundamental resonance frequency is observed when the film thickness is an integral multiple of the half of the wavelength of the signal. At resonance a sharp change in electrical impedance is occurred. Now this resonant frequency depend on the many factor like the thickness of the electrode, fabrication technique (because residual in structure causes the scattering of wave in other direction and also require a good c - axis orientation), external electric field which generate the initial stress in the system and shift the resonant frequency. Dimensions of the FBAR should be ½ the wavelength in longitudinal direction and 50-ohms filter design for network matching.

For generation of acoustic wave the common method is to use the piezoelectric material and its effect can be accounted as

$$\boxed{\begin{aligned} S &= sT + d^E E \\ D &= \varepsilon E + d^s T \end{aligned}}$$

where S is strain, D is dielectric displacement, T is stress, E is electric field, d is electromechanical coefficient, s^E is compliance effect with electric field, ε^S and is the permittivity with effect of strain.

The transduction process requires the electrical field to the piezoelectric material, which is done by using the electrodes or the close proximity to the surface of the piezoelectric material. A small size electrode is attached to the piezo material for contact with air so the acoustic waves are reflect back and energy confined in the system. If a big size of electrode is used then air gap between the piezolayer and electrode is needed but this introduces a series capacitance and reduces the piezoelectric coupling by a factor of

$$c = \frac{1}{1 + c_T / c_G}$$

where c_T is plate capacitance and c_G is the gap capacitance.

The series and parallel resonance will be occurred. At series resonance the impedance is very low and is only resistive. The frequency below the series resonance the current flow is capacitive and above it, the current flow is inductive. At parallel resonance, the impedance is very high and for frequency above parallel resonance the current flow is again capacitive. Technology driving forces *are* cost effective (cell phone market-its filter cost and battery requirement), performance (high frequency operation), device size (smaller as possible). The strength of piezoelectric coupling determines the bandwidth of filter and mechanical losses in material determine the quality factor (Q) and accordingly the insertion losses. All the frequency of RF band now used by the cell phones communication and other government agencies so the more unique range of frequency need to be find so not to get interfered with other frequencies.

1.2 History

The free standing FBAR is first demonstrated in 1980 by Grudkowski et al. and independently that same year by Nakamura, et al. In 1982, Lakin et al give a paper which emphasizing the future potential of FBAR and mainly the size and the performance. The first book on FBAR is written by Rosenbaum in 1988. ZnO is the early material choice because one can easily sputter them. AlN sputtering was introduced in 1981 by Wang and Lakin. That time the AlN sputtering is not easy, but AlN is compatible with the IC technology while ZnO can't. In 1993, HP started research on the FBAR and the main focus was on the Molybdenum (Mo) and Tungsten (W) as electrode and AlN as piezoelectric layer and good success were found with Mo. The main focus was that what should be the device fabrication process, i.e. bulk etching or surface etching.

The early research on FBAR in HP lab was not well supported because SAW technology was at high volume production and it was a one mask process. In 1998, the duplexer was made and wired in the first working cell phone to make calls to upper management. The ceramic duplexer was replaced by the FBAR duplexer. With the use of FBAR, the new generation of smaller and thin cell phone came to market.

1.3 Piezoelectric and Pyroelectric properties

Pyroelectric properties

This is the ability of the certain materials to generate a temporary voltage when they are heated or cooled. Temperature modifies the position of the atom slightly and polarization takes place. If the new temperature remains constant, then the generated voltage will disappear because of the leakage of current. This current leakage is in the crystal or in the air or through the voltmeter connected across it. This property is different from the thermo-electric property because the set up of thermo-electric effect uses the 2 different materials

connected and provide two different temperatures. Also, there is no leakage current in thermoelectric effect.

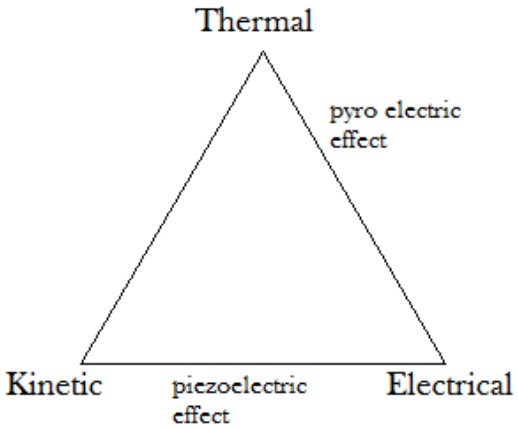

Figure 1-3 Different effects in material

Pyroelectric coefficient can be given as $P_i = \frac{\partial P_{S,i}}{\partial T}$ where it shows changes in spontaneous polarization vector with temperature. Pyroelectric charge generated at the different faces but direction remains constant. This direction can only be changed by nearby electric field. All the materials that have pyroelectric property also have the piezoelectric properties, but vice versa are not true because some of the piezoelectric material has the symmetrical structure. There are 32 different classes of crystal according to their rotational axis and reflection plane. 21 classes of crystal do not have the centre of symmetry and so posses the piezoelectric properties. 20 of them have the direct piezoelectric properties and 10 out of these 20 are having the pyroelectric property. These 10 are having polarities i.e. they possess a spontaneous polarization and having dipole in their unit cell.

Piezoelectric properties

Piezoelectric effect is the property of a material to convert the mechanical energy into the electrical energy and vice-versa. The main criterion of piezoelectric effect is the lack of centre of symmetry. The piezoelectric effect is shown through the figure below.

Let  shows the Al ions and  shows the N ions. And let they form the structure

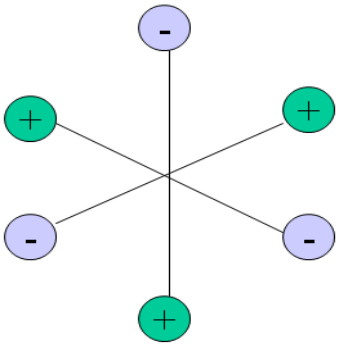

Figure 1-4 Ions placement in molecule

When a compressive or tensile force applied to the piezoelectric material then an electric charge is produced on the opposite surface and can be picked up using electrodes. When the stress generated in the system, it causes a strain too, and the strain directly Proportional to the stress i.e. $T \propto S$ or

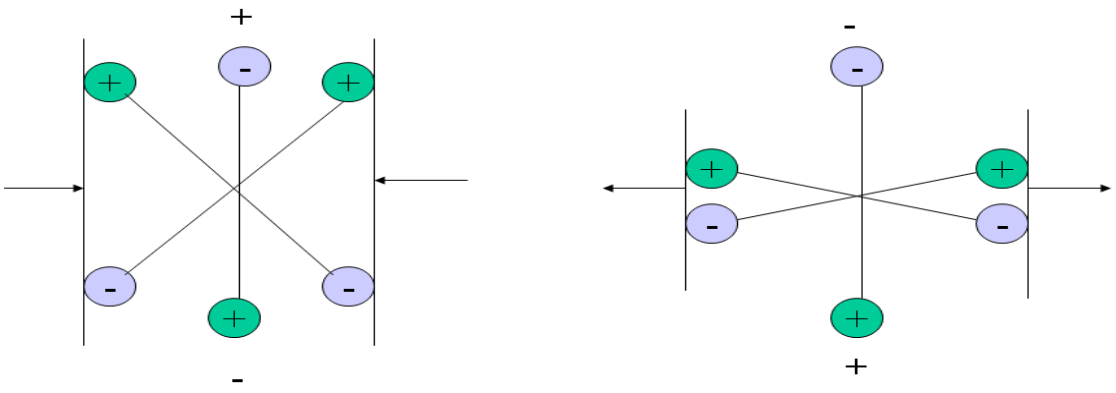

Figure 1-5 Ions adjustment after applying compressive and tensile strength

$$T = cS \tag{1.1}$$

$$\frac{1}{c} = s$$

$$S = sT \tag{1.2}$$

where c is stiffness (young's modulus of elasticity) and inverse of stiffness is called compliance. It forms a capacitive structure and its capacitance can be given as

$$C = \frac{\varepsilon A}{t}$$

And also Q=CV

$$\text{So, } Q = \frac{\varepsilon AV}{t}$$

Electric density displacement D can be given as D=Q/A, put the value of Q,

$$\boxed{D = \frac{\varepsilon AV}{At} = \frac{\varepsilon V}{t} = \varepsilon E} \tag{1.3}$$

The equation 1.3 is only true for the isotropic material. Piezoelectric materials are isotropic only when they are in a non polarization state, but in the polarized state they are non-isotropic and each direction have different effect and so the equation modified as

$$D_i = \varepsilon_{ij} E_j$$

$$\begin{bmatrix} D_1 \\ D_2 \\ D_3 \end{bmatrix} = \begin{bmatrix} \varepsilon_{11} & \varepsilon_{12} & \varepsilon_{13} \\ \varepsilon_{21} & \varepsilon_{22} & \varepsilon_{23} \\ \varepsilon_{31} & \varepsilon_{32} & \varepsilon_{33} \end{bmatrix} \begin{bmatrix} E_1 \\ E_2 \\ E_3 \end{bmatrix}$$

The changes occur in D is due to the electric field in the same direction and the rest of the directions will be showing a zero effect and so the coefficient. The non-zero coefficients are $\varepsilon_{11} = \varepsilon_{22}, \varepsilon_{33}$.

Piezoelectric effect on constants

In the piezoelectric device, due to the conversion of mechanical to electrical and vice versa, their corresponding coefficient will be modified i.e.

- Dielectric constant vary with mechanical load

$$\varepsilon_{r(clamped)} = \varepsilon_{r(free)}(1+K^2) \tag{1.4}$$

- Stiffness constant vary by an electrical field

$$\gamma_{open}(1+K^2) = \gamma_{shorted} \tag{1.5}$$

K is the coupling factor which is used to evaluate the quality of the electromechanical conversion of a piezoelectric material. This constant shows the efficiency of energy conversion from electrical to mechanical and vice versa.

The conversion between the electrical domain to mechanical and mechanical to electrical is represented by a coefficient given as d_{ij} (electromechanical conversion). Due to this effect, there will be some modification occur in the hook's equation

$$\begin{aligned} S_i &= s_{ij}^E T_j + d_{ik} E_k \\ D_i &= \varepsilon_{ij}^S E_j + d_{ik} T_k \end{aligned} \tag{1.6}$$

$$\begin{bmatrix} S_1 \\ S_2 \\ S_3 \\ S_4 \\ S_5 \\ S_6 \end{bmatrix} = \begin{bmatrix} s_{11} & s_{12} & s_{13} & 0 & 0 & 0 \\ s_{21} & s_{22} & s_{23} & 0 & 0 & 0 \\ s_{31} & s_{32} & s_{33} & 0 & 0 & 0 \\ 0 & 0 & 0 & s_{44} & 0 & 0 \\ 0 & 0 & 0 & 0 & s_{55} & 0 \\ 0 & 0 & 0 & 0 & 0 & s_{66} \end{bmatrix} \begin{bmatrix} T_1 \\ T_2 \\ T_3 \\ T_4 \\ T_5 \\ T_6 \end{bmatrix} + \begin{bmatrix} 0 & 0 & d_{13} \\ 0 & 0 & d_{23} \\ 0 & 0 & d_{33} \\ 0 & d_{42} & 0 \\ d_{51} & 0 & 0 \\ 0 & 0 & 0 \end{bmatrix} \begin{bmatrix} E_1 \\ E_2 \\ E_3 \end{bmatrix}$$

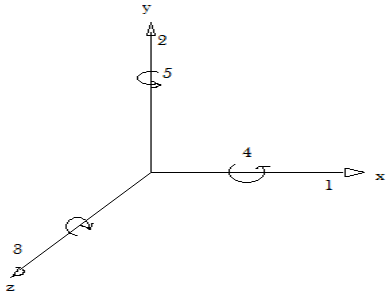

Figure 1-6 Axis for stress and strain

$$\begin{bmatrix} D_1 \\ D_2 \\ D_3 \end{bmatrix} = \begin{bmatrix} 0 & 0 & 0 & 0 & d_{15} & 0 \\ 0 & 0 & 0 & d_{24} & 0 & 0 \\ d_{31} & d_{32} & d_{33} & 0 & 0 & 0 \end{bmatrix} \begin{bmatrix} T_1 \\ T_2 \\ T_3 \\ T_4 \\ T_5 \\ T_6 \end{bmatrix} + \begin{bmatrix} \varepsilon_{11} & 0 & 0 \\ 0 & \varepsilon_{22} & 0 \\ 0 & 0 & \varepsilon_{33} \end{bmatrix} \begin{bmatrix} E_1 \\ E_2 \\ E_3 \end{bmatrix}$$

These matrices forms are used for the calculation of all the parameters in 3D.

1.4 Applications

- *RF filter and duplexer*
  - As frequency spectrum is limited and favorable frequencies are occupied by cell phones communication, government agencies etc so some new frequency need to be used.
  - The RF filter bandwidth required is small and steep for the communication without interference.
  - Before FBAR, dielectric and waveguide filters are used which have ohmic losses, skin effect, eddy current in metal conductor and provide very low quality factor (Q).
  - Acoustic wave store and carry energy very efficiently than electromagnetic waves in air.
- *Oscillator*
  - FBAR can be used as an oscillator for above 2GHz frequency because it has very high value of quality factor (Q) and can be maintained up to 5GHz. This will eliminate frequency doubler and PLL.
  - Temperature compensation can be obtained by SiO_2
  - It can be electrically tuned to a specific frequency
- *Sensor*
  - By using a special coating FBAR can be used as chemical and biological sensor
  - A mass loading effect used for the sensor
  - Deformation sensor
  - Inertial sensor
  - Ultraviolet light detector
  - Biological sensor

1.5 Motivation

- Tools and process available today for semiconductor device manufacturing have reached to a level so that a good quality structure can be achieved and with effective cost.
- There is an option for monolithic integration of microelectronics and bulk acoustic device.

- There is a space of research work on optimization of the parameters of the FBAR like material, fabrication process, tuning etc.
- FBAR frequency shift and high quality factor (Q) value have explored the new application in the sensing system.
- Due to FBAR commercial success, it is important to make the device more optimize and introduce new capabilities in the device.

1.6 Outline of thesis

This thesis work is having the analytical analysis and designing and simulation of the FBAR device in order to find the application areas.

Chapter 2 covers the basics of the resonator device. In this chapter the full 2D derivation of the resonator, coupling coefficient, quality factor, topologies and the tuning techniques are discussed. A simple prototype is selected to study the effects in the resonator for the different condition. Loss mechanisms are also explained. The equivalent electrical model Butterworth van dyke (BVD) of the FBAR is also discussed.

Chapter 3 covers the literature review on the FBAR device in which the different application and recent development are mentioned. Also the comparison of the piezoelectric material and the electrode material are shown. FBAR is compared with some of its competitive filters in this chapter.

Chapter 4 cover the designing part of the FBAR which is used in the simulation and the different simulation condition and the basic boundary conditions are shown in this chapter. Also the results and their familiar responses are shown in the chapter.

Chapter 5 have the results calculated analytically by using the derived formulas in the chapter 2. Also the simulated results are shown in this chapter. All the results are compared and the discussion on the results is in this chapter.

Chapter 6 has fabrication and characterization of the layers of the aluminium nitrite. The characterization shows the content of the material and the transmission and absorption characteristics through the sample.

Chapter 7 has the conclusion of the present work and the scope for the future work.

Chapter 2 Resonator theory

2.1 Basic physics of resonator

In this chapter, the study of the crystal's acoustic properties is done by developing the fundamental mechanical equations in one dimension. When an unbalance system of time varying stresses applied to the crystal then it results in propagating of an acoustic waves in the crystal and these waves propagate with the velocity which is depend on the crystal material properties. This one dimensional relation can easily be extended in the 3 dimension by using the stress and strain 3D matrixes in its linear relations.

In static cases, the stresses are equal because there is no net motion of any internal volume but in dynamic cases where the waves are propagating, the opposite stresses are not generally equal. Assume that 1 and 2 are close masses and they are ΔL distance apart as shown in figure 2.1, which is small enough that also write it as $\Delta L = dz$ and the unbalance forces are applied to the both of the end causes the strain in the structure. The new distance between the particles become Δl

$$dF_1 = dAT_1$$
$$dF_2 = dAT_2$$
$$u_1 \neq u_2$$

Through the following statement, the strain is written as

$$S = \frac{\partial u}{\partial z} \tag{2.1}$$

Newton's law

$$\partial F = m * a$$
$$dF = \frac{\partial T}{\partial z}\partial z * dA$$

Compare this and above equation and we get the relationship between stress and particle displacement

$$\frac{\partial T}{\partial z} = \rho \frac{\partial^2 u}{\partial t^2} \tag{2.2}$$

$$\frac{\partial T}{\partial z} = \rho \frac{\partial v}{\partial t} \tag{2.3}$$

Now by using equation (1) and hook's law, we get

$$\frac{\partial v}{\partial z} = \frac{1}{c}\frac{\partial T}{\partial t} \tag{2.4}$$

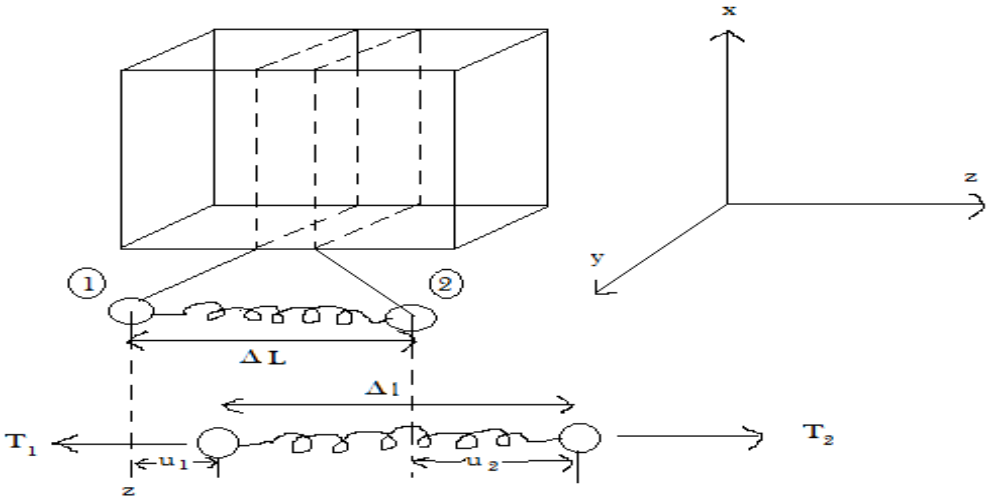

Figure 2-1 Simple cubic structure in tensile force

Differentiate equation 3 and 4 with respect to z and t resp. and compare them together,

$$v_a = \sqrt{\frac{c}{\rho}} \tag{2.5}$$

This is the phase velocity which depends upon the stiffness and the density of the material and can be easily find out by material properties. In the acoustic system the particle displacement is not in the phase with the particle velocity. Let the displacement can be given as

$$u = u_0 e^{j(\omega t - \beta z)} \text{ ----- } (a)$$

Differentiate this with respect to the z and we will get the strain

$$S = \frac{\partial u}{\partial z} = -j\beta u \tag{2.6}$$

The phase relation between S and v, to find the value of v from the equation (a) and we get $v = j\omega u$. Now, this equation with the equation (6) becomes

$$S = -\frac{\beta v}{\omega} \tag{2.7}$$

From equation (2.6) and (2.7), the T and S are in the same phase and all others are 90^0 out of phase with the 'u' and 180^0 out of phase with 'v'.

Acoustic impedance (z) is very important properties of piezoelectric materials. Acoustic impedance is given as the ratio of the stress to the velocity of particle in the material and can be written as

$$z = -\frac{T}{v} = -\frac{cS}{v}$$
$$= \frac{(-c)(-ju\beta)}{v}$$
$$= \frac{juc\omega}{v * v_a}$$
$$z = \sqrt{\rho c} \tag{2.8}$$

This acoustic impedance is also depending on the basic material properties.

Absorption of an acoustic wave

If the solid material obeys the hook's law very precisely then there would be no acoustic absorption in the materials, but in the real world, there are viscous damping forces and non-linearity in the material which causes energy to be extracted from the wave in the form of heat. So these forces can be included by modifying the hook's law

$$T = cS + \eta \frac{dS}{dt}$$

where last part shows the damping coefficient and derivation shows that the strain tends to relax with time towards the equilibrium. Also

$$\frac{\partial T}{\partial z} = \rho \frac{\partial v}{\partial t}$$

Now, put the value of T and differentiate with respect to t

$$\frac{\partial^2 (cS + \eta \dot{S})}{\partial t \partial z} = \rho \frac{\partial^2 v}{\partial t^2}$$

This can be expanded and the square derivative value of S is replaced with the equivalent value of v, then we get

$$c\frac{\partial^2 v}{\partial z^2} + \eta \frac{\partial^3 v}{\partial z^2 \partial t} = \rho \frac{\partial^2 v}{\partial t^2} \tag{2.9}$$

If in this equation, put the value of damping ratio equal to zero then get basic equation. Now assume a general complex propagation function of velocity

$$v = Ae^{j(\omega t - \hat{k}z)}$$
$$where...\hat{k} = \beta + j\alpha$$

Now find the value of different derivative of the general function

$$\frac{\partial^2 v}{\partial t^2} = -\omega^2 v$$
$$\frac{\partial^2 v}{\partial z^2} = -\hat{k}^2 v$$

Put both value in equation (9) and then expand the value of by expanding the values

$$-c\hat{k}^2 v - j\eta\omega\hat{k}^2 v = -\omega^2 \rho v$$
$$-\omega^2 \rho = -c(\beta^2 - \alpha^2 + j2\alpha\beta) - j\eta(\beta^2 - \alpha^2 + j2\alpha\beta)$$

Take the real part only and equate the equation

$$-\omega^2\rho = -c\beta^2 + c\alpha^2 + 2\eta\beta\alpha\omega$$

2nd and 3rd part are neglected (α) because of vary small values and so we get

$$v_a^2 = \frac{c}{\rho} = \frac{\omega^2}{\beta^2}$$

Now just take the imaginary part and solve it

$$\alpha = \frac{\eta\beta\omega}{2c} = \frac{\eta\omega^2}{2v_a^3\rho} \tag{2.10}$$

α Variable can be given in terms of Q factor also

$$\alpha = \frac{\omega}{2Qv_a}$$

$$Q = \frac{v_a^2\alpha}{\omega\eta}$$

Power in the system

In the acoustic system, total power can be found out as the kinetic energy and the strain energy and the losses occur in the system. In the acoustic system, the power can be given as the multiplication of the stress and the velocity of the system. The equation can be given as

$$-\frac{\partial(Tv)}{\partial z} = -\frac{\partial(\frac{1}{2}\rho v^2 + \frac{1}{2}cS^2)}{\partial t}$$

This is the equation for the lossless system. The first term on the right hand side is particle kinetic energy density and the second term is the strain energy density. If the system is having losses, then equation needs to be modified as

$$-\frac{\partial(Tv)}{\partial z} = -\frac{\partial(\frac{1}{2}\rho v^2 + \frac{1}{2}cS^2)}{\partial t} - \frac{1}{2}\frac{\partial}{\partial t}(\omega\eta S^2)$$

Through the power relation, quality factor can easily be deducted by the system

Q = [ω (power stored)/dissipated energy per cycle]

$$Q = \frac{cS^2}{\omega\eta S^2}$$

$$Q = \frac{v_a^2\rho}{\omega\eta} \tag{2.11}$$

2.1.1 Prototype of resonator

The equations are used for the piezoelectric material are as follows:

$$T = c^E S - eE$$

$$D = eS + \varepsilon^s E$$

Now these equations can be further solved by putting the value of E in previous equation and the equations will become

$$T = c^E(1+\frac{e^2}{c^E\varepsilon^S})S - \frac{eD}{\varepsilon^S} \tag{2.12}$$

From the equation (2.12), the phase velocity detected as

$$v_a^D = \sqrt{\frac{c^D}{\rho}}$$

$$= \sqrt{\frac{c^E}{\rho}}\sqrt{1+K^2}$$

And so

$$v_a^D = v_a\sqrt{1+K^2} \tag{2.13}$$

This equation shows the first effect of the piezoelectric material in the system, i.e. acoustic velocity is higher than it was detected from c^E and from the above equation (2.13), get the electromechanical coupling coefficient K^2

$$K^2 = \frac{e^2}{c^E\varepsilon^S} \tag{2.14}$$

It measures the conversion efficiency of the piezoelectric material from mechanical to electrical and electrical to mechanical. Now move further to see the effect on a simple prototype for some real life consequences. Some assumption before move further and that are as follows:

- Assume thickness of the piezoelectric layer is 2d
- Mass less electrode covering opposite faces of the piezolayer
- Also assume that lateral dimensions are much higher

Now let take a general Ansatz for displacement

$$u(z,t) = [a\sin(kz) + b\cos(kz)]e^{j\omega t}$$

where k = wave no.

a & b is a constant determined by boundary condition

$$\frac{\partial^2 u}{\partial t^2} = \frac{c^D}{\rho}\frac{\partial^2 u}{\partial z^2}$$

so

$$\omega^2.u(z,t) = \frac{k^2c^D}{\rho}.u(z.t)$$

$$k = \frac{\omega}{v^D}$$

$$k = \frac{\omega}{v^D} = \frac{2\pi}{\lambda} \tag{2.15}$$

So wave number can be given as the ratio of angular frequency to the phase velocity.

In the similar fashion the stress component is calculated and for the simplicity just drops the time factor of the equation.

$$T(z) = c^D k[a\cos(kz) - b\sin(kz)] - \frac{eD}{\varepsilon^S} \tag{2.16}$$

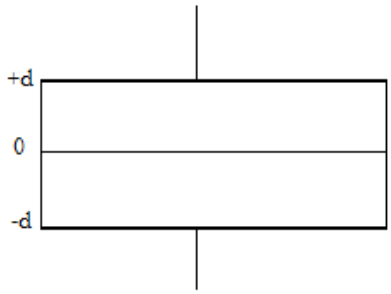

Figure 2-2 Simple structure of FBAR

By applying the boundary condition to the device as the stress outside the device must be zero i.e. $T(\pm d) = 0$. Solving eq. 5 by applying the boundary condition, we get a value of constants as b=0 and $a = \frac{eD}{\varepsilon^D c^D k} \frac{1}{\cos(kd)}$. Now put these values of constant in the eq. (5)

$$T(z) = \frac{eD}{\varepsilon^D}\left[\frac{\cos(kz)}{\cos kd} - 1\right] \tag{2.17}$$

The equation is calculated for the stress and put this stress equation (6) in the equation (1)

$$\frac{\partial u}{\partial z} = \frac{eD}{c^D \varepsilon^S} \frac{\cos(kz)}{\cos(kd)}$$

$$k(a\cos(kz) - b\sin(kz)) = \frac{eD}{c^D \varepsilon^S} \frac{\cos(kz)}{\cos(kd)}$$

As we have calculated that b=0

$$a\cos(kz) = \frac{eD}{c^D \varepsilon^S k} \frac{\cos(kz)}{\cos(kd)}$$

Now put the value of the constant in the function of u(z)

$$u(z) = \frac{eD}{c^D \varepsilon^S k} \frac{\sin(kz)}{\cos(kd)} \tag{2.18}$$

In order to find the response of the system to the outside electrical stimulus, we need to rearrange the equation of stress, strain, electric field and dielectric displacement as

$$E = \left[\frac{1}{\varepsilon^S} - \frac{e^2}{c^D \varepsilon^{2S}}\right] D - \frac{e}{c^D \varepsilon^S} T \tag{2.19}$$

Voltage can be found out at the boundary of the electrode by using the electric field equation

$$V = \int_{-d}^{+d} E(z)dz$$

$$V = \frac{2dD}{\varepsilon^S}\left[1 - \frac{e^2}{c^D \varepsilon^S} \frac{\tan(kd)}{kd}\right] \tag{2.20}$$

The current can be derived from the electric displacement factor

$$I = j\omega A.D$$

The impedance can easily be calculated as

$$Z = \frac{V}{I} = \frac{1}{j\omega C_0}\left[1 - K_t^2 \frac{\tan(kd)}{kd}\right] \tag{2.21}$$

Here $C_0 = \frac{\varepsilon^S A}{2d}$ is the capacitance of the device

$$K_t^2 = \frac{e^2}{c^D \varepsilon^S} \tag{2.22}$$

This is called the electromechanical coupling factor for the thickness longitudinal vibration. Now by using the impedance equation, the resonant and anti-resonant frequencies of the system can be found out. At the anti-resonant frequency, the impedance of the system is infinite and at resonant frequency, the value of impedance is very low i.e. almost zero. In resonant mode all the impedance is only resistive.

Case 1: when z=∞ i.e. anti resonant frequency

$$kd = (2n+1)\frac{\pi}{2}$$

Put the value of k i.e. wave no here

$$\omega_{a,n} = (2n+1)\frac{\pi}{2}\frac{v^D}{d} \tag{2.23}$$

Case 2: when z=0 i.e. resonant frequency

$$\frac{1}{K_t^2} = \frac{\tan\left(\frac{\pi}{2}.\frac{\omega_r}{\omega a,0}\right)}{\left(\frac{\pi}{2}.\frac{\omega_r}{\omega a,0}\right)}$$

$$K_{eff}^2 = \frac{\frac{\pi}{2}\frac{f_S}{f_p}}{\tan\left(\frac{\pi}{2}\frac{f_S}{f_p}\right)} \tag{2.24}$$

This equation can further simplifies as

$$K_{eff}^2 = \frac{\pi^2}{4}\frac{f_S}{f_p}\left(\frac{f_p - f_S}{f_p}\right)$$

We can also write it as

$$1 = K_t^2 \frac{\tan(\frac{\theta}{2})}{\frac{\theta}{2}}$$

Now expand the tangent function

$$\tan\left(\frac{\theta}{2}\right) = \frac{4\theta}{\pi^2 - \theta^2}$$

$$8K_t^2 = \pi^2 - \theta^2$$

$$\omega_r = \frac{v_a}{2d}\left(\pi^2 - 8K_t^2\right)^{\frac{1}{2}} \tag{2.25}$$

2.1.2 Coupling coefficient

Coupling coefficient gives the efficiency of the energy conversion from the electrical to mechanical and mechanical to electrical in the piezoelectric device. In the earlier discussion, it is concluded that the coupling coefficient of material and device both are different. K^2 is the piezoelectric material coupling coefficient i.e. it shows the property of the materials that certain materials are intrinsically better for making the electro acoustic conversion than others. For example PZT has much higher K^2 than AlN.

On the other hand k_{eff}^2 is the property of the whole device. K^2 influence what kind of effective coupling might be expected from a manufactured device. By using definition of k_{eff}^2, this is having a volume V,

$$U = \frac{1}{2}\int (TS + ED)dV$$

$$U = U_e + 2U_m + U_d$$

In the equation, U_e is elastic energy, U_m is mutual energy, U_d is the electrical density.

$$U_e = \frac{1}{2}\int_V \frac{U_m^2}{U_e U_d} \tag{2.26}$$

In equation 2.26, on the right side numerator part show the interaction of stress and electric field through coefficient "d" and their coupling. Denominator part is showing the total energy stored in the system.

The simple form of energy can be given as

$$U_e = \frac{1}{2}\int_V (Ts^E T)dV$$

$$U_m = \frac{1}{4}\int_V (TdE + EdT)dV$$

$$U_d = \frac{1}{2}\int_V (E\varepsilon^T E)dV$$

Till now, the assumption is that the electrode thickness is negligible, but in the real case it is not possible to neglect the electrode thickness. So boundary condition is changed as well i.e. $T(\pm(d+t)) = 0$, where t is the electrode thickness.

$$k_n(d+t) = (2n+1)\frac{\pi}{2}$$

$$\omega_{a,n} = (2n+1)\frac{\pi}{2}\frac{v}{d+t}$$

As seen the wave number and anti resonant frequency is modified and will also modified the coupling coefficient as boundary condition changes and after solve for these boundary condition with same procedure ended up with the equation as

$$k_{eff}^2 = \frac{e^2}{\varepsilon^S c^E} \frac{8}{\pi^2} \frac{\cos\left[(2n+1)\frac{\pi}{2}\frac{t}{d+t}\right]}{(2n+1)^2\left[1-\frac{t}{d+t}\right]} \tag{2.27}$$

For n = 0, 1, 2.....

Representation of the eq. 2 in the graphical form for the value of n = 0,

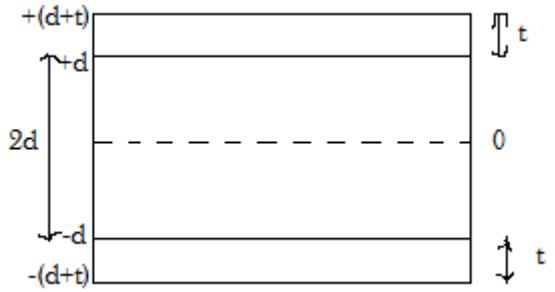

Figure 2-3 Resonator with electrode of finite thickness t

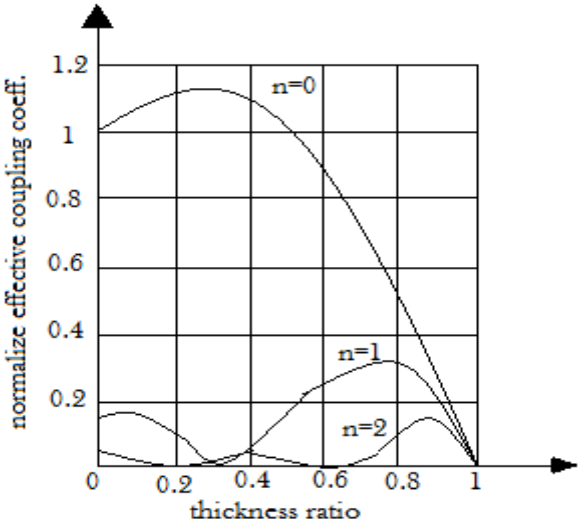

Figure 2-4 Thickness to the normalized coupling coefficient

The coupling coefficient has the maximum value for thickness ratio at the value of 0.26. Also for the n=0, the coupling coefficient is high and for other harmonics it is very low. The electrode and piezolayer do not have the same properties so more realistic situation, the displacement is considered in 2 different parts.

$$u(z) = \begin{Bmatrix} a\sin(k_p z)\, for - d \le z \le +d \\ b\sin(k_e z + \gamma)\, for, z > d \end{Bmatrix}$$

The following graphs show the effect of impedance difference and the velocity difference of the electrode from the piezoelectric layer.

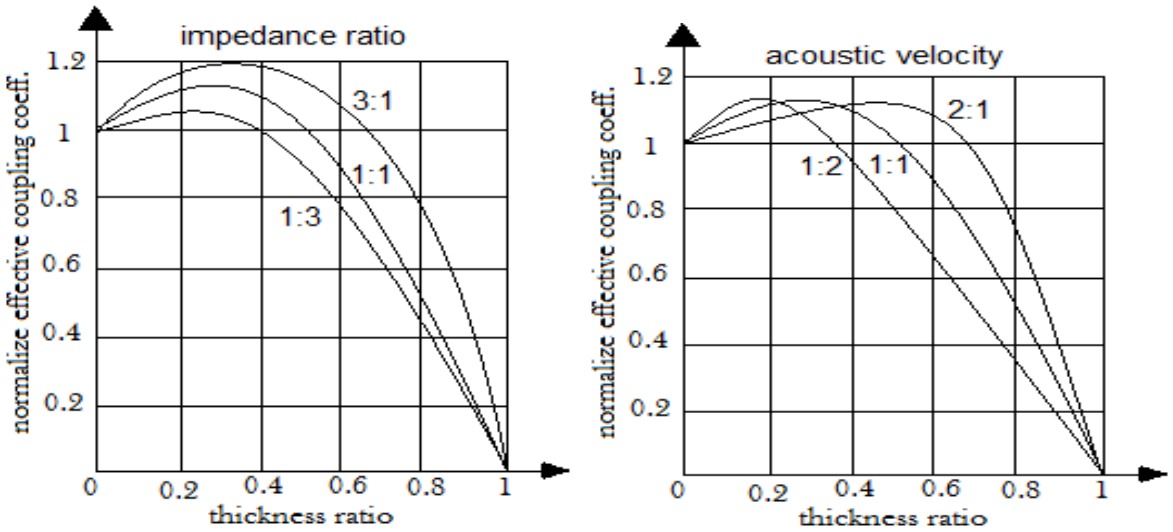

Figure 2-5 Electrode thicknesses to normalized coupling coefficient (a) with variable impedance ration (b) with variable acoustic velocity

Figure 2.5(a) shows that when the impedance of the electrode decrease, then the coupling coefficient also decreases, so the coupling coefficient is directly proportional to the impedance of the electrode. The second figure 2.5(b) shows that if the acoustic velocity of electrode is less than the piezoelectric layer, then less thickness of electrode is required, which is very difficult to fabricate.

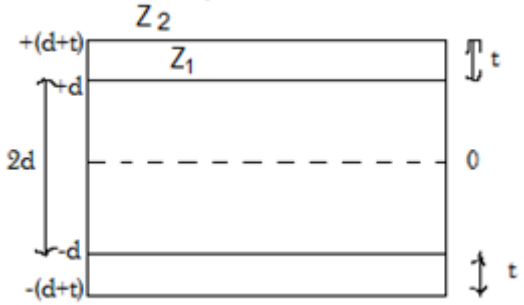

Figure 2-6 Electrode with impedances

Electrode works here as a reflector of energy. Z_2 is acoustic impedance of air and Z_1 is the acoustic impedance of the electrode. When an acoustic wave meets an interface will cause the reflection and refraction. Transmission must be very low and reflection should be very high.

$$\text{Transmission coefficient } t = \frac{2Z_2}{Z_2 + Z_1}$$

$$\text{Reflection coefficient } r = \frac{Z_2 - Z_1}{Z_2 + Z_1}$$

$$\text{So concluded that } Z_1 >> Z_2$$

2.1.3 Loss mechanism and Quality factor (Q)

Strength of piezoelectric coupling determines the bandwidth of the filter and mechanical losses determine the Q factor and filter insertion losses. The structure of the device plays a very important role in determining the losses etc of the device. Electrode thickness is very important for the coupling and losses in the device. Electrode resistance is a very important

factor in metallisation. At series resonance, the current is large, so losses through the resistance of electrode increase while thicker metal lower the resistance but increase mechanical losses. So in between there is an optimum metal thickness of the whole resonator design. Q factor can be given as if there are multiple losses in the system

$$\frac{1}{Q_{total}} = \sum \frac{1}{Q_i}$$

Here Q_i are the values associated with the loss mechanism. The losses which may be contributed to the Q must be gas damping, thermo elastic damping, acoustic radiation losses through anchors and others.

$$\frac{1}{Q} = \frac{1}{Q_{gas}} + \frac{1}{Q_{TED}} + \frac{1}{Q_{anchor}} + \frac{1}{Q_{others}}$$

Thermo elastic is the irreversible process of strain energy to the thermal energy and anchor losses occur when elastic energy is transferred from the device to the substrate through the anchor. So most of the energy propagate to the package and the board and is not recoverable.
Structural damping is caused by crystallographic defects like dislocation and grain boundaries that affect the propagation of the stress wave through the material. Acoustic losses are expected when the acoustic wave crosses over from one material to another. Damping is the property of material and structure influence the dynamic response. Mass and stiffness proportional damping, which are generally referred to as Rayleigh damping are used in nonlinear dynamic analysis.

$$\xi = \frac{\alpha}{2\omega_n} + \frac{\beta\omega_n}{2} = \frac{1}{2Q}$$

If the value of Q at 2 different frequencies is known then both the constants can be found.
There are number of losses location in the device which is as follows:

1. **Electrical losses**
   It is associated with the finite resistance of resonator's electrodes and connection leads. The electrodes required with high acoustic impedance which also has low resistance. But some metals are good i.e. their resistance do not increase as the size decrease to very low level e.g. Al, Cu, Ag, Au etc.
   Another resistive part arises from the possible non uniform stress distribution over the area of the electrode, when the resonator operating at high frequency. If stress distribution is not flat, then areas of the resonator will vibrate at different amplitude and phase and will redistribute current associate with them and cause the eddy current formation and have a resistance and so ohmic losses started and this decrease the Q value of the device. Eddy current formed by varying the magnetic field, creating by RF current driving in BAW (Lorentz law). The resistivity of the conductor acts to damp the amplitude of eddy current and thus eddy current create losses through heating.

2. **Acoustic attenuation**
   It is the phenomenon where some of the mechanical energy propagates in the material is converted into heat.

3. **Leaking wave**
   In FBAR, the lower and upper surfaces are in the contact with the air and hence high acoustic mismatch. So it can be certain that no wave transmitted to the air and consequently in the substrate. Shear wave velocity is half of the longitudinal wave velocity. And if somehow the shear wave generated, then it will cause the Q factor to reduce but these are very small. The origin of these shear waves can be any non perpendicular longitudinal wave that reflects and transmitted in the device. Lateral leaking waves propagate in the outside of the region and lower the Q value and effective coupling.
4. **Spurious modes**
   The narrow band effect will be causing the impedance and phase of a resonator to deviate around the main resonance. They cause the standing wave. These waves can be terminated by proper edge finishing. The suppression helps in smoothing the curve and reduces filter losses and increase Q. These modes can also be removed by the topologies.
5. **Viscoelastic losses**
   In Viscoelastic material, when load is applied, energy is stored and when load is removed, all the energy is not recovered and some of it lost in the form of heat. In this the cyclic strain applied and the stress is not in the phase and will have a difference say ϕ, this angle is directly proportional to the damping. Viscoelastic materials are dependent on many properties like frequency, temperature, dynamic strain rate, time effect like a creep and relaxation.
6. **Scattering losses**
   These losses occur in the layer of the material, i.e. interface roughness and lateral device boundary roughness, which causes the waves in the lateral direction and produce losses.

2.1.4 FOM

Quality factor and effective coupling are the closely related variables that show the quality of the device. Both of them need to be at optimum value and so there combine and optimum result is shown by the factor figure of merit (FOM). FOM is given as

$$FOM(f) = k_{eff}^2 * Q(f)$$

Coupling coefficient does not vary with the frequency change and changes are very little with changes in the design so we have very less flexibility to change it. Q factor can be changed and so to increase FOM we need to increase the quality factor. FOM can also be measured using smith chart i.e. a measurement of resistance at series and parallel frequency will give the FOM.

$$R_p \approx FOM(f_p) * X_0$$

$$R_s \approx \frac{X_0}{FOM(f_s)}$$

$$where, X_0 = \frac{1}{\omega C_0}$$

2.2 Electrical equivalent models

2.2.1 Butterworth van-Dyke model (BVD)

The equivalent model of the FBAR can be modelled by Butterworth Van-Dyke model (BVD). The different components are assigned as

- Vibrating mass (motional inductor), L_m
- Elasticity of piezoelectric material, C_m
- Mechanical losses, R_m
- Electrode form a static parallel plate capacitance, C_0

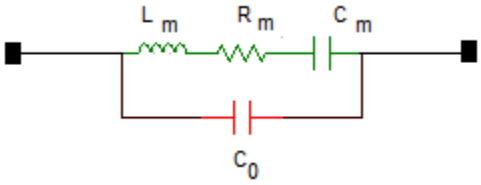

Figure 2-7 BVD equivalent model

Series and parallel frequency can be calculated by this equivalent circuit and the equation is given as

$$f_s = \frac{1}{\sqrt{L_m . C_m}}$$

$$f_p = f_s (1 + \frac{C_m}{C_0})$$

Figure of merit can be given in the terms of capacitance also

$$FOM = \frac{Q}{(\frac{C_0}{C_m})}$$

This model does not include some part of the FBAR and so a modified version of BVD is used and this is represented as

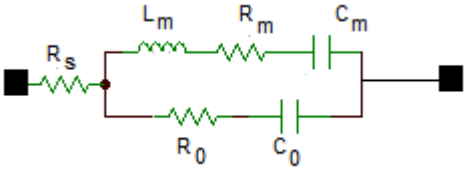

Figure 2-8 Modified BVD model

Here, R_0, R_s are dielectric/ohmic losses and transmission losses respectively. All the components can be given in the form of resonant frequency and the capacitance of the FBAR structure.

$$C_0 = \frac{\varepsilon A}{d} \qquad C_m = C_0 \left[\left(\frac{f_p}{f_s} \right)^2 - 1 \right] \qquad L_m = \frac{1}{(2\pi f_p)^2 C_m} \qquad R_m = \frac{1}{2\pi f_s C_m Q}$$

2.3 Temperature effects and compensation

Most materials have the negative temperature coefficient for stiffness i.e. they get softer as temperature increase and affect the acoustic resonator. Quartz is a unique material because it has the positive temperature coefficient and stretched because of the stretching of Si-O chain. There are no piezoelectric material have the temperature compensation property for the resonator so the use of composite layering of piezo layer and SiO_2 layer (SiO_2 has positive temperature coefficient).

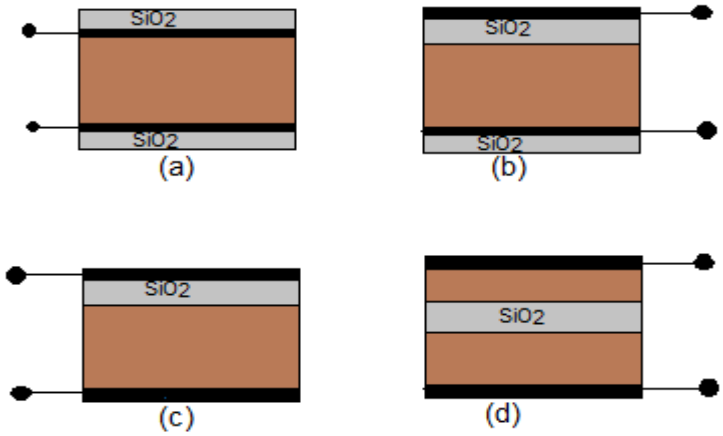

Figure 2-9 Various configuration for temperature compensation

Figure 2.9 (b) is good for the Al because Al gets the good orientation over silicon oxide. Figure 2.9 (b, c and d) have the silicon oxide in between the resonator area and causes resonator to act as a series of capacitor and this will lead to the reduction of coupling coefficient. While the figure 2.9 (a) does not have the silicon oxide in between and so does not make any series capacitance. But here on upper electrode, the silicon oxide increase the weight and this will cause the resonant frequency to shift down and also there is the depositing problem of pinning of silicon oxide over aluminium. Temperature coefficient of frequency (TCF) varies as the dimensions change and which causes the resonant frequency to be changed. The TCF is an important factor and can be given as

$$\frac{1}{\omega}\frac{d\omega}{dT} = \frac{1}{2}\left(\frac{1}{C}\frac{dC}{dT} - \frac{1}{\rho}\frac{d\rho}{dT}\right) - \frac{1}{d}\frac{dd}{dT}$$
$$= \frac{1}{2}\left(\frac{1}{C}\frac{dC}{dT} + \frac{1}{V}\frac{dV}{dT}\right) - \frac{1}{d}\frac{dd}{dT} \qquad (2.28)$$

On the right hand side, the first term shows the change in stiffness which is already discussed is the negative coefficient of temperature. The second term is a volumetric thermal expansion coefficient (α_V) and third term shows the linear thermal expansion coefficient α_l. In isotropic cases, $\alpha_V > 3\alpha_l$ and both cancel each other in the equation (1) so the overall effect left is $\frac{1}{2}\alpha_l$ and the value of this lies between 1 to 20 ppm/K. Temperature coefficient of stiffness constant are typically in the range of a few tens to few 100 off ppm/K. So it is the largest effect on determining the TCF. So ultimately the TCF should be low. SiO_2 has a positive

temperature coefficient and can be used to offset the effect of -25ppm/^{0}C temperature coefficient of AlN.

SiO_2 has +85ppm/^{0}C

AlN has -25ppm/^{0}C

So use the thickness of SiO_2 so that the AlN temperature coefficient is reduced. The oxide layer is softer than AlN and electrode so it affects the Q value.

2.4 Apodization and Tuning

Apodization term refers to changing the shape of a mathematical function of an electrical signal, an optical transmission or a mechanical structure. It is also called tapering or a window function to smoothly bring a sampled signal down to zero at the edge of the sample region i.e. suppresses the leakage side lobes. Apodization or loading the upper electrode reduces the spurious effect.

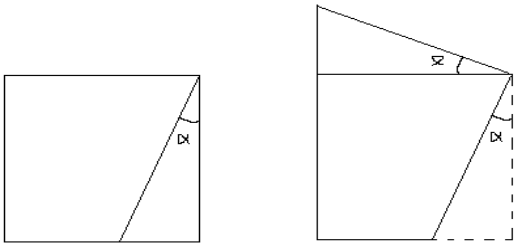

Figure 2-10 Apodization

To suppress the spurious modes, make the sides anti-parallel. If it has the parallel side, then the leakage wave will make the standing wave, but for non parallel sides, multiple reflections do not form constructive wave and so lose less energy. As α increase, spurious mode decrease.

For many applications, it is not possible to get the exact perfect resonant frequency. So to get that frequency there is number of ***tuning process***.

- The post process technique is mass loading and widely used. Metal fuse and evaporation used by heating FBAR. But unfortunately this is a onetime process.
- Electrical tuning offer a great variation in the resonant frequency and so used in VCO. When a DC voltage is applied i.e. an initial biasing voltage then this voltage changes the resonant frequency because initially make the stiffness in the device.
- Another method is by embedded the heater and by using the temperature variation, we can easily vary the resonant frequency. But this method is not good for device life.

Note: - The area of the FBAR is used to vary the impedance of the device to make it adjustable with the communication system having 50ohms impedance.

2.5 Topologies

There are 2 very popular topologies widely used

2.5.1 Ladder filter

It is the filter having the FBAR connected in the ladder form as shown in the figure.

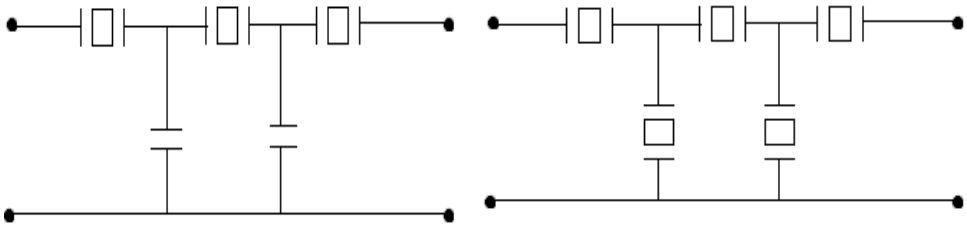

Figure 2-11 (a) capacitor in parallel branch, (b) FBAR in both the branches

This topology transmits maximum power to the output so it needs to reduce the resistance of the series component and increase the impedance of the parallel branch. In figure (a) capacitor is used as in the parallel branch and so this configuration has high value of Q for the low frequency as the reactance of capacitor is high for low frequency. While in the second configuration, the parallel branch FBAR, as it has the high impedance at parallel resonance. So tune in such a way that parallel resonant frequency becomes equal to the series resonance of the FBAR in series branch. In this situation, the maximum power can get at output and no power will go to the ground, because all the current will only flow through the series branch. The shifting of frequency can be done by any tuning method discussed earlier or use the inductor in the parallel branch.

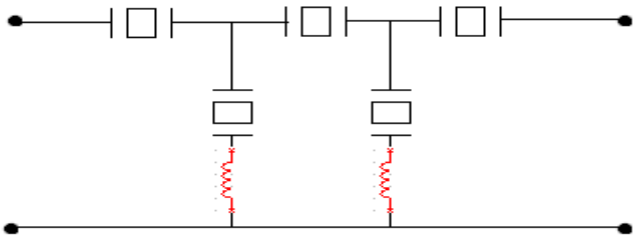

Figure 2-12 Shifting of parallel branch resonant frequency by the inductor

The ladder topology has very steep rejection response and it is good for blocking the signal close to the pass band but poor at rejecting undesired band.

2.5.2 Lattice filter

With the increasing interest for high frequency application where in the direct connection with RF IC's is done best with balance network.

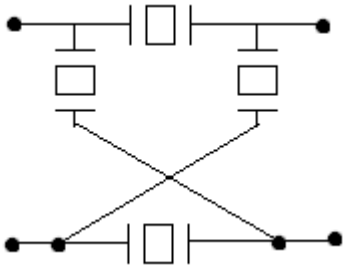

Figure 2-13 Lattice configuration

Lattice filter suppresses the pole zero response and give the multi pole response. Lattice topology is not good at removing the signal near pass band, but more effective in rejecting undesired band.

Chapter 3 Literature and material properties

3.1 Literature Review

S.V. Krishnaswamy *et al.* [36] demonstrated the film bulk acoustic resonator (FBAR) technique. A 2 pole monolithic ladder filter in the operating range of 1-1.5GHz has been demonstrated. The size of the device taken as 0.3x0.3x0.02 inch and having the bandwidth of 30MHz at 1GHz resonant frequency and insertion losses of 1dB. In this paper, a comparison of the FBAR with other filter was shown. The comparison is on the bases of the insertion losses and the size of the device where the FBAR posses the lowest size and the insertion losses as well. The technique i.e. fabrication, temperature compensation and monolithic processing was demonstrated. Also the issue related to integration of FBAR with the action circuits, IC processing compatibilities etc. were also addressed.

Giwan Yoon *et al.* [37] demonstrate a 2 step sputtering deposition technique for the piezoelectric layer deposition on the electrode layer and utilize this technique for the FBAR devices. ZnO film was used for the sputtering. The ZnO piezoelectric film is sputtered over the Au layer by using the RF magnetron sputtering. The highly c-axis orientation was achieved over the electrode layer and this c-axis orientation was utilized for the FBAR as it provided very high electromechanical coupling coefficient. The quality factor achieved of 7235. It was also demonstrated that the impedance matching can be achieved by changing the area of the electrode.

Qingming Chen *et al.* [38] demonstrate the relation between the quality factor and the electromechanical coupling coefficient. The relation between the Q and coupling coefficient was inversely proportional. It has been found that the quality factor affects the coupling coefficient as the Q increase, the coupling coefficient decreases up to a level and then stabilizes. Coupling coefficient also depends on the thickness of the layer and also the properties of the material. The combination of the layers also affects the coupling coefficient. The thickness ratio affects the coupling coefficient as shown in the chapter 2. The study was carried out by using the 1D transfer matrix method.

K.M Lakin *et al.* [39] demonstrated the fabrication and the designing technique for the wide band gap filters. It was used for the GPS and the wireless LAN application using the coupled resonator. The stacked crystal filter was used for the high performance application where higher degree of band attenuation was required. Active area of 265x265μm was used. The combination of the ladder filter with the stack crystal filter (SCF) and the coupled resonator filter (CRF) was demonstrated. SCF and CRF are coupled to get the wide band gap with the high ultimate rejection. Channing of SCF/CRF with the ladder filter can be used to obtain the best of the both of the filter.

Wei Pang *et al.* [40] demonstrate the self aligned lateral field excitation film bulk acoustic resonator and achieved an electromechanical coupling coefficient of 10% at 4.1 GHz with the quality factor of 35. In this resonator, the improved energy trapping structure has been demonstrate that does not require an electrode gap to micron and utilize the simple 2 mask

process for fabrication that eliminate the misalignment between the piezoelectric ZnO and metal electrode. A new processing technique to clearly show ZnO film through the lift off without any wet etching also demonstrated.

Mathios Link *et al.* [41] demonstrate the solidly mounted film bulk acoustic resonator which was operating at 850 MHz in the shear vibration mode. The coupling coefficient for the ZnO film is achieved of 1.7% and the quality factor of 312 in the external air environment. In fabrication the micro fluidic channels are made with the FBAR. The device was placed in the liquid environment and the large changes in the quality factor were detected. Quality factor reduced to 192 from 312 for the water liquid environment. This makes the FBAR a good candidate for the biosensors. Also the device is demonstrated with the liquid of 59% Glycerol and a change of 136 from 312 in the quality factor was detected.

Linh Mai *et al.* [42] demonstrate the design and fabrication of the ZnO based film bulk acoustic resonator (FBAR) by employing a new type of Bragg reflector with a very thin chromium layer formed between the silicon oxide and tungsten. The device showed a very good return losses and very high quality factor. 3 different designs were studied with the same configuration by changing the bottom supporting layer thickness and the top electrode pattern was also changed.

Wei Pang *et al.* [43] was demonstrated the design, fabricating and measurement of the electrically tunable film bulk acoustic resonator (FBAR). The device was formed by electrostatic micro electro-mechanical system actuator. The tuning of 1.47% was achieved at the 1.5 GHz frequency by applying the voltage of 7V. The FBAR and air gap capacitance integration was done. The quality factor achieved was 304. Two different electrode designs were used with top electrode air gap and form capacitor on a side. This works as the varactor and changed the resonant frequency. The applied voltage varied from 10.8 to 27.2 Volts and a shift in resonant frequency was detected. The tuning technique demonstrated the possibility to obtain the zero temperature compensation.

Xu Zhang *et al.* [44] demonstrated the thermal analysis and characterization of film bulk acoustic resonator (FBAR) as the biosensor in liquid environment. A quality factor of 120 was achieved. The sources of thermal effect were analyzed. The temperature coefficient of frequency (TCF) of -112 ppm/K for the uncompensated circuit and it was reduced to 1ppm/K by applying a properly chosen bias to the oscillator and suggest the possibilities of the feedback to achieve thermal stability. Fabrication of microfludics channel was done by using the material parylene. For the different thickness of ZnO films, the experiment was carried out and changes in the quality factor were collected.

J. Oiler *et al.* [45] demonstrated the enhancement in the sensitivity of the radiation sensor based on film bulk acoustic resonator (FBAR). The new design and materials selection was carried for the experiment. The parallel resonant frequency of the FBAR after irritation due to radiation induced charge trapping in silicon nitrite SiN. Two layers of silicon nitrite were used to increase the sensitivity by over 2 orders of magnitude. The sensitivity of 2300

KHz/Krad was achieved. Different thicknesses of silicon nitrite were experimented and good results are collected at the thickness of 0.3μm.

Luis Garcia Gancede *et al.* [46] demonstrated the ZnO based film bulk acoustic resonator with the electrode of carbon nanotube (CNT). These CNT were fabricated using the thermal chemical vapour deposition technique. CNT posses the very low density and very high acoustic impedance which reduces the mass loading effect and better confinement of standing waves of acoustic propagation. CNT has the significant effect on the attenuating travelling wave on the surface of the FBAR. The return losses are 5dB smaller at resonance. The quality factor of around 1000 was achieved. It was concluded that CNTs were an excellent electrode but for the bottom layer they are not the best candidate because they do not lead to a good orientation of piezoelectric layer.

Abhay Kochhar *et al.* [47] demonstrated the integration process for the fabrication of the film bulk acoustic resonator (FBAR) over the CMOS IC. The adhesion bonding was used to transfer the silicon in the CMOS chip. Benzocyclobutene (BCB) was used as the adhesion layer which is stable at 300^0 C. CMOS was protected by BCB and makes it safe from plasma and chemicals. Transferred silicon offered flat surface and FBAR was fabricated on the silicon and then back etched for suspension. The ruthenium and aluminium used as the top and bottom electrode respectively. Monolithic FBAR-CMOS integration process for the VCO application was used. CMOS die area was rough so BCB adhesion used with silicon and then fabricated over it.

3.2 Comparison of FBAR and SAW

SAW is the major element of filter RF frequency and is in the mass production. This technology is older than the FBAR and also lots of research work going on the SAW and this make it a good competitive device to FBAR. SAW and BAW cover the whole RF market. SAW does not used for high frequency because the electrode pitch requires is narrow and so require fine lithography of electrode in nano range, which increase the resistance of the electrode and the Q value become so low. Other filters like an LC filter which has more parasitic effect and these effects cannot be neglected at the frequency above 0.8GHz. Transmission line filters have very large size and losses and the ceramic filters are good, but not fabricated on silicon and form monolithic device.

Table 3-I Comparison of FBAR and SAW technology

FBAR	SAW
Utilize C-axis orientation of AlN or ZnO	It uses $42^0$4 $LiTaO_3$ as the substrate
Vibrate in thickness extension (TE) mode	Vibrate in shear horizontal (SH) mode
Central frequency determined by thickness of piezoelectric material	Central frequency is determined by the pitch of the electrode
High Q factor, particularly in the high frequency range	Very suitable in the low frequency application (below 2GHz)
High power durability and resistance to electrostatic discharge (ESD)	It is not a bulk device so not having good power durability
The possibility of realizing monolithic device with the active RF device	Substrate is less compatible with monolithic device
Require more mask and fabrication steps	Few steps process and cost effective
Wave guided in higher velocity region	Wave guided in slower velocity region

3.3 Piezoelectric and electrode materials comparison

3.3.1 Piezoelectric materials

3.3.1.1 Zinc oxide

- It is easily deposited by RF sputtering
- As device reaches to higher frequency, its acoustic losses also increased
- High TCF
- Not CMOS compatible
- ZnO quickly absorbs the moisture and increase losses
- Band gap is 3.37eV and lattice constants are a=3.249 $\overset{0}{A}$ and c=5.207 $\overset{0}{A}$
- It has the wurtzite structure

3.3.1.2 PZT

- Very high coupling coefficient
- It posses both piezo and pyroelectric property
- High acoustic losses at high frequency so used in low frequency application
- It have very low Q value

3.3.1.3 Aluminium nitrite

- Very high velocity of sound in C-axis
- Very high young's modulus and high thermal conductivity
- Relatively low TCF
- AlN is stable compound with a strong covalent and ionic bond
- Bonding energy is 11.5eV and band gap is 6.2eV
- Wurtzite crystalline structure with hexagonal symmetry
- Lattice constants are a=3.11 $\overset{0}{A}$ and c=4.978 $\overset{0}{A}$

Table 3-II Properties in comparison of piezoelectric material

Material	AlN	ZnO	PZT	Units
Acoustic velocity	11.05	6.35	4.6	10^3m/s
Young's modulus	3.94	2.11	0.49	10^{11}N/m^2
Piezoelectric coefficient (d_{33})	5.6	12.4	200	10^{-12}C/N
k_{eff}^2	6.5	8.5	35	%
Thermal conductance	320	60	1.8	W/mK
TCF	-25	-60	-	Ppm/^{0}C
Dielectric constant	8.5-9.5	9.2	80-400	
Insertion loss	Very low	Low	high	

3.3.2 Electrode material

For a good orientation of electrode, bottom layer of the electrodes must be in good orientation or use CMP to reduce roughness to 0.70 nm because it controls the piezolayer orientation. The electrode must have low resistance to the compatible standard manufacturing technique. Its acoustic impedance and stiffness determine the acoustic wave penetrates in the electrode before it reflects back. If stiffness is high, then losses are less and less electrode penetration. Gold and copper are rejected due to their poor acoustic stiffness. Al is a good conductor, but having a low acoustic impedance compared to W, Mo. Cu is used for interconnects because its conductivity is 1.5 times the Al and acoustic impedance, same as Al but the worse Q value. W is difficult to be deposited as a low stress film. Mo and AlN form a good combination.

Table 3-III Acoustic properties of various electrode materials

Material	Density (g/cm^3)	Sonic velocity (10^3m/s)	Acoustic impedance	Stiffness (10^{11}Pa)
AlN(002)	3.26	11	3.6	4.2
SiO_2	2.2	5.6	1.2	0.7
Pt	21.5	3.96	8.474	3.5
Al	2.7	6.3	1.7	1.1
Mo	10.2	6.2	6.4	-
W	19.2	5.2	10	-
Cu	8.9	4.7	4.2	-

- Aluminium
  - Available easily
  - Low resistance
  - Moderate coupling coefficient
- Molybdenum
  - High stiffness and moderate resistance
  - Thermal expansion is similar to AlN and so no residual stresses
- Tungsten

- Higher acoustic impedance and high stiffness
- thermal expansion is similar to AlN
- Have very high coupling, but heavier so resonant frequency is less

- Platinum
  - Best film to orient AlN
  - Withstand with high oxidation
  - Very high coupling coefficient
  - Get very low resonant frequency and low Q factor

Table 3-IV Physical properties of various electrode materials

Material	Bulk resistivity (micro ohms-cm)	Thermal expansion (ppm)	Thermal conductivity
Al	2.8	22.9	2.3
Pt	10.7	8.9	0.716
Mo	5.7	5.1	1.38
W	5.39	4.3	1.73
Ti	22	8.9	0.46
Ru	7.3	9.6	1.17

3.4 Piezoelectric constants of AlN and ZnO

3.4.1 AlN piezoelectric constant

Table 3-V AlN piezoelectric constants

Elastic constant (10^{11}N/m^2)	
c_{11}	3.45
c_{12}	1.25
c_{13}	1.20
c_{33}	3.95
c_{44}	1.18
c_{66}	1.10
Piezoelectric constant (C/m^2)	
e_{15}	-0.48
e_{31}	-0.58
e_{33}	1.55
Dielectric constant (10^{-11}f/m)	
ε_{11}	8
ε_{33}	9.5

3.4.2 ZnO piezoelectric constant

Table 3-VI ZnO piezoelectric constants

Elastic constant ($10^{11}N/m^2$)	
c_{11}	2.097
c_{12}	1.211
c_{13}	1.051
c_{33}	2.109
c_{44}	0.424
c_{66}	0.443
Piezoelectric constant (C/m^2)	
e_{15}	-0.1134
e_{31}	-0.543
e_{33}	1.32044
Dielectric constant ($10^{-11}f/m$)	
ε_{11}	8.5446
ε_{33}	10.204

Chapter 4 Design and simulation

4.1 CoventorWare

CoventorWare is an industry standard simulation tool for design of Micro-electro-mechanical systems (MEMS) and modelling of Semiconductor and MEMS manufacturing process. This tool enables designers to simulate and optimize MEMS device designs and fabrication process before committing to time consuming and costly build and test cycles.

Procedure to simulate:

1) Write a process file
2) Enter/modify material properties
3) Draw 2D layout design
4) Generate 3D solid model
5) Name faces and mesh the model
6) Apply boundary conditions
7) Apply model to solver
8) Display results

Analyzer module is used to simulate the FBAR behaviour with the different electrodes. Simulation is carried out to examine:

1) FBAR resonant frequencies (series and parallel)
2) Quality factor magnitude and phase
3) Capacitance, displacement and Mises Stresses
4) Impedance
5) Harmonic displacement and phase

The structure of FBAR consists of a silicon substrate, thermally generated silicon oxide, electrode layer, a piezoelectric layer of aluminium nitride and an electrode layer over it. Different electrode used in this simulation. A process file is written in the process editor and a layout is generated in layout editor which imitate device fabrication and lithographic steps.

A solid 3D model is generated and meshed with extruded brick elements. Meshing is a method of breaking the big structure into a set of finite small elements. Prior to meshing, faces are given meaningful names so that proper boundary conditions can be applied for simulation. During device fabrication, Silicon substrate and thermal dioxide are used as a platform for fabrication only and their role in device operation is insignificant thus they are not considered in the simulation. FBAR's 3D model and its meshing model are shown in the figure 4.1 and 4.2.

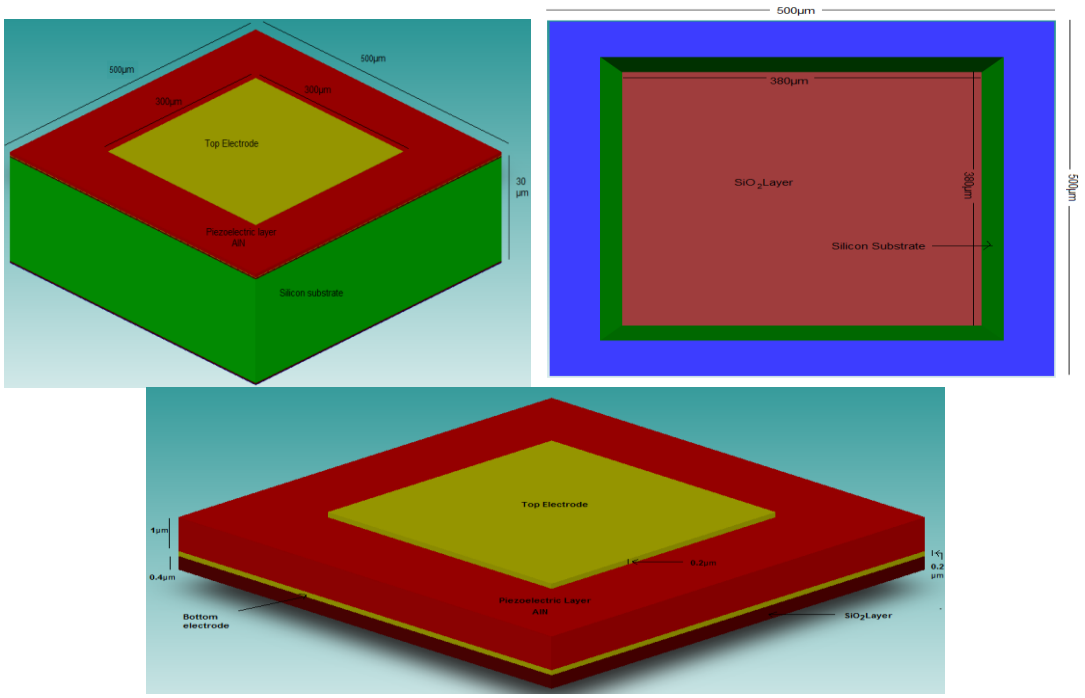

Figure 4-1 Design of the simulated FBAR

Different materials are used during the simulation of the FBAR. Electrode material properties used for the simulation are given in the table 4.1. Properties used for the AlN are already given in the chapter 3.4.1.

Table 4-I Material properties used

Electrode material	Density (g/cm3)	Poisson's ratio	Young's modulus	TCE	Thermal conduction
Aluminum	2.3	0.3	7.7	2.31	2.4
Platinum	2.14	0.35	1.45	8.9	7.16
Tungsten	1.93	0.27	4.1	4.5	1.78
Molybdenum	1.03	0.31	3.29	4.8	1.38

4.2 Capacitance, Displacement and Mises Stresses

Simulation for finding the capacitance is done using the MemMech solver in the MEMS domain of the CoventorWare. In MemMech solver, physics used is piezoelectric. The DC analysis is run for the capacitance finding. It has the top and bottom electrode and top electrode is put on 1 V and the bottom electrode at the ground. The dimensions of the active device are 300 x 300 x 1.3 µm. The thickness is distributed as 0.15 µm for top and bottom electrodes and 1µm for the piezoelectric layer. This configuration is over a silicon dioxide layer 0.18 µm thick, which is thermally grown on a silicon substrate of 30 µm.

Table 4-II Capacitances for different electrode configuration

AlN with electrodes	Capacitance (pF)
Platinum	9.49375
Aluminium	9.498057
Tungsten (T) and aluminium (B)	9.493472
Molybdenum	9.48563

The displacement generated by the voltage applied to the electrode is simulated and shows the different values for the different electrode configuration. The displacement is shown in the figure 4.3.

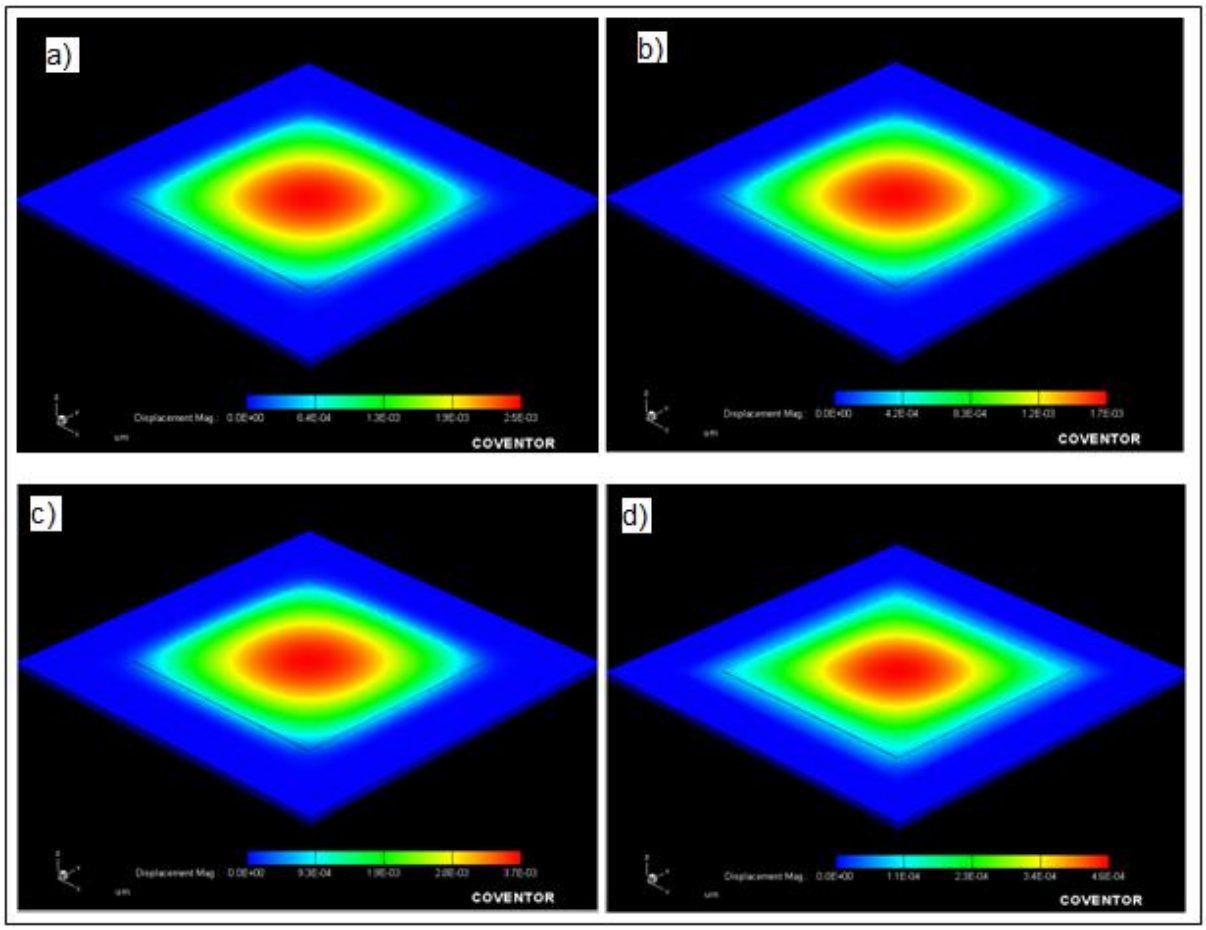

Figure 4-2 Displacement in device for different electrodes a) platinum, b) aluminium, c) Molybdenum, d) Tungsten

The Mises stress generated in the device is of magnitude of 1.2 Mpa for each of the electrode configuration.

4.3 Modal analysis

Modal analysis of the FBAR is done in the MemMech module to find the resonant and anti-resonant frequencies. In the MEMS domain study, the physics applied is piezoelectric in which the additional analysis is done by using modal analysis. Different modes of frequency are visualized and the resonant frequency is selected which find the behaviour is as like

shown in the figure 4.4. The vector must be coming out as the parallel to the surface. As seen the maximum magnitude is in the centre. The series analysis for the FBAR with the four different electrode configurations is shown in table 4.3 and the parallel resonance is shown in the table 4.4.

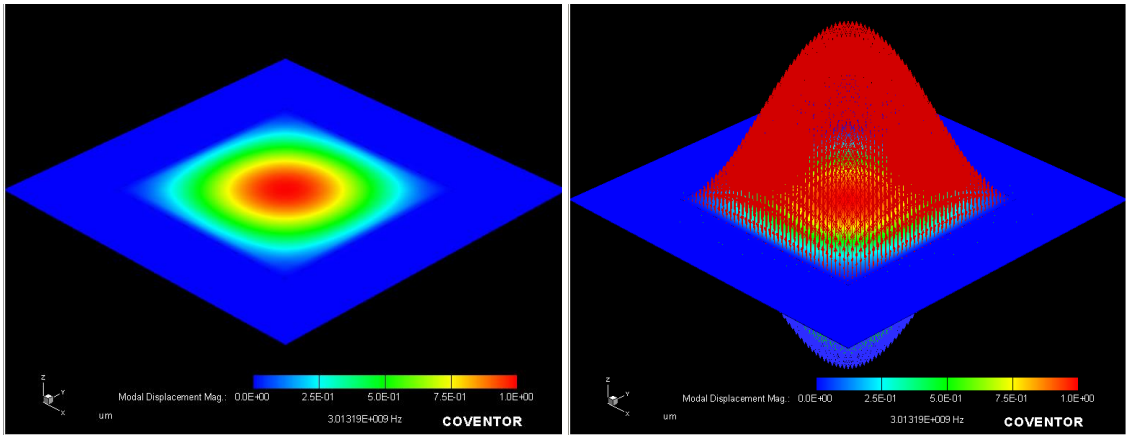

Figure 4-3 Response of the resonance and vector field

Table 4-III Series resonant frequency for different electrode configuration

AlN with electrodes	Series resonant frequency (GHz)
Platinum	2.17167
Aluminium	4.4903
Tungsten (T) and aluminium (B)	3.2705
Molybdenum	3.01319

Table 4-IV Parallel resonant frequency for different electrode configuration

AlN with electrodes	parallel resonant frequency (GHz)
Platinum	2.2314
Aluminium	4.62334
Tungsten (T) and aluminium (B)	3.3597
Molybdenum	3.1024

4.4 Quality factor and impedance

Quality factor is the important factor of FBAR. Simulation for finding the quality factor is done by using the MemMech solver. In MEMS domain, the piezoelectric physics is used. The direct modal analysis is done for the quality factor. In the range of resonant frequency, the simulation is run to find the quality factor. The simple and harmonic boundary conditions are

given according to the device. The quality factor obtains for the same design for the all different electrode configurations. The quality factor is seen in the figure 4.5.

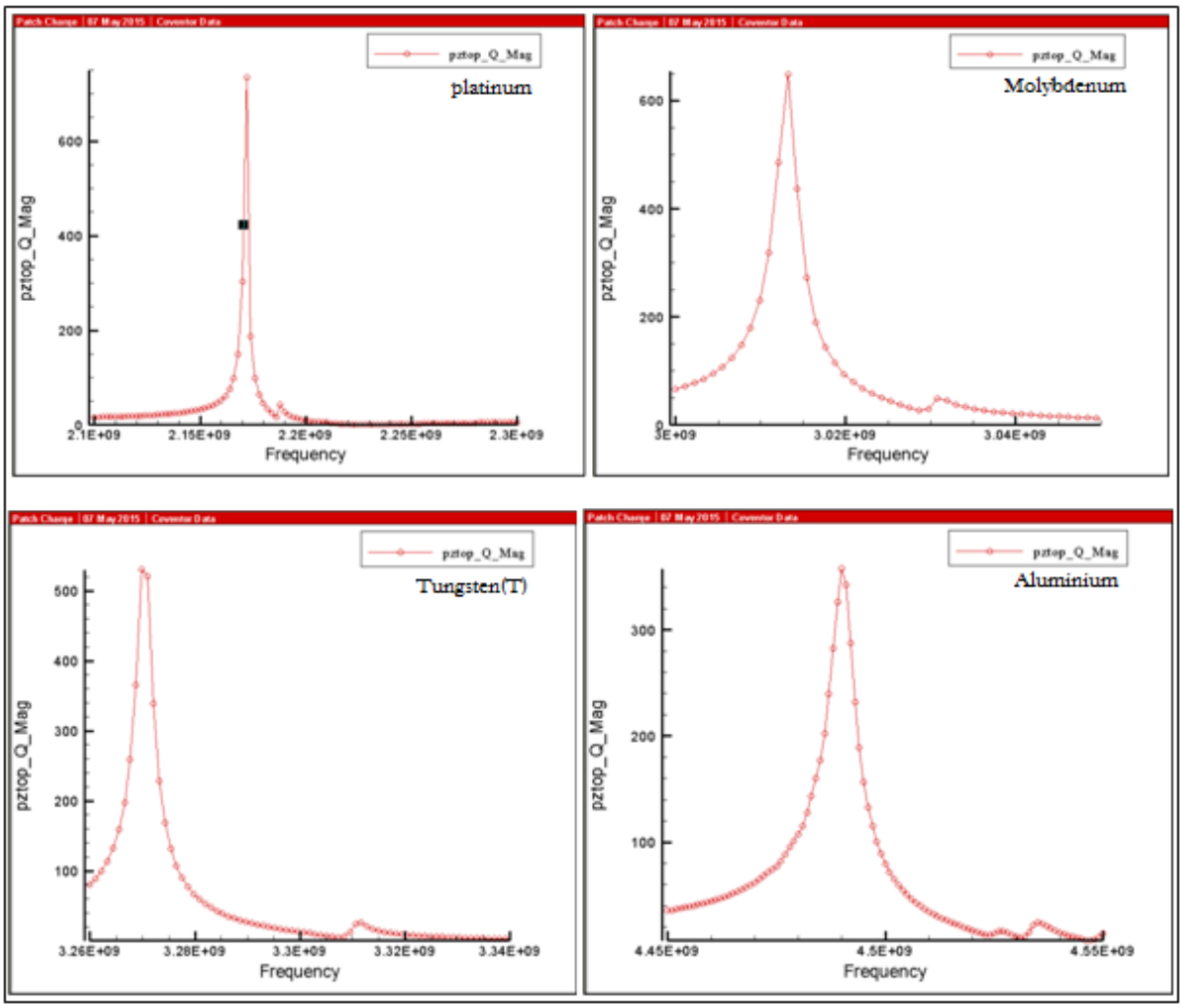

Figure 4-4 Responses of the quality factor magnitude

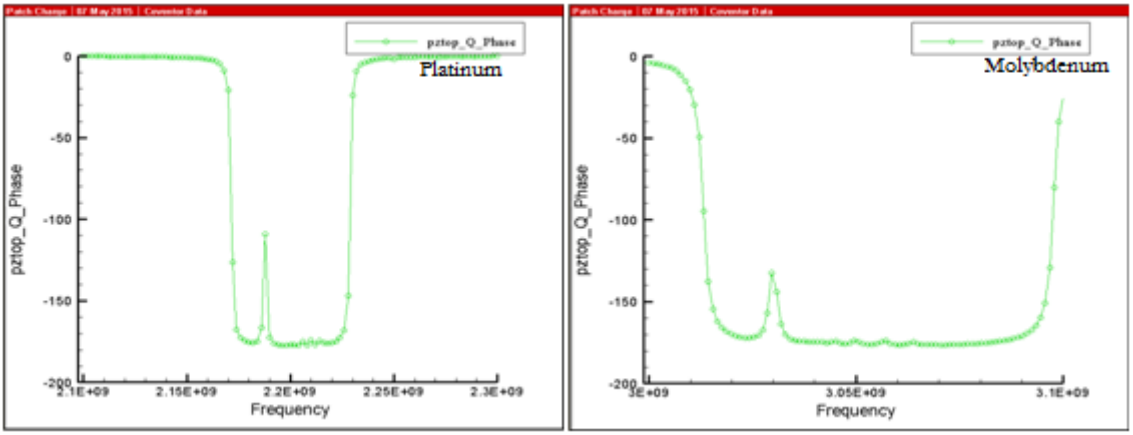

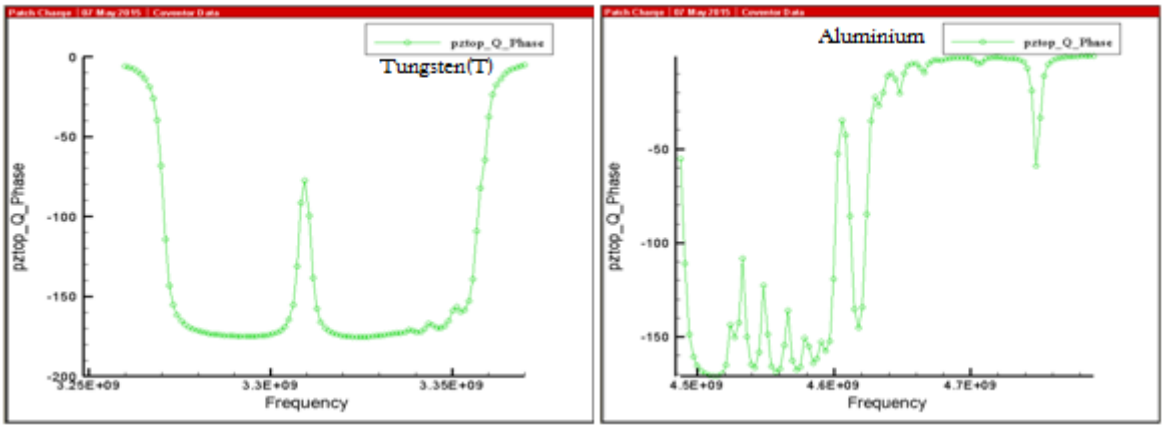

Figure 4-5 Responses of the quality factor phase

As seen from the figure, the responses of the quality factor for the different electrode. The maximum value of quality factor obtained at series resonance. The value of the quality factor's maximum value at resonance is given in the following table.

Table 4-V Quality factors

AlN with electrodes	Quality factor
Platinum	735.5
Aluminium	360
Tungsten (T) and aluminium (B)	530.5
Molybdenum	650

The impedance of the FBAR is calculated from the same simulation results. It indicates the change in the impedance of the FBAR with the change in the frequencies. It is very helpful to visualize that the amount of losses in the system i.e. if the graph of impedance shows the large variation between the resonant frequency, then the losses are higher. As we see in the aluminium impedance response, which shows large variation and so the losses, whereas the response for the platinum is very smooth and so the less losses.

In these equations, the angular frequency is calculated by using the simulated result. The real and imaginary parts of the quality factor are calculated from the polar form solution of the quality factor in the simulation. Using the these, the real and imaginary part of the impedances are found out and then the rectangular form is converted into the polar form and the response can be seen in the graph form. The values have already been simulated for the requirement of these equations.

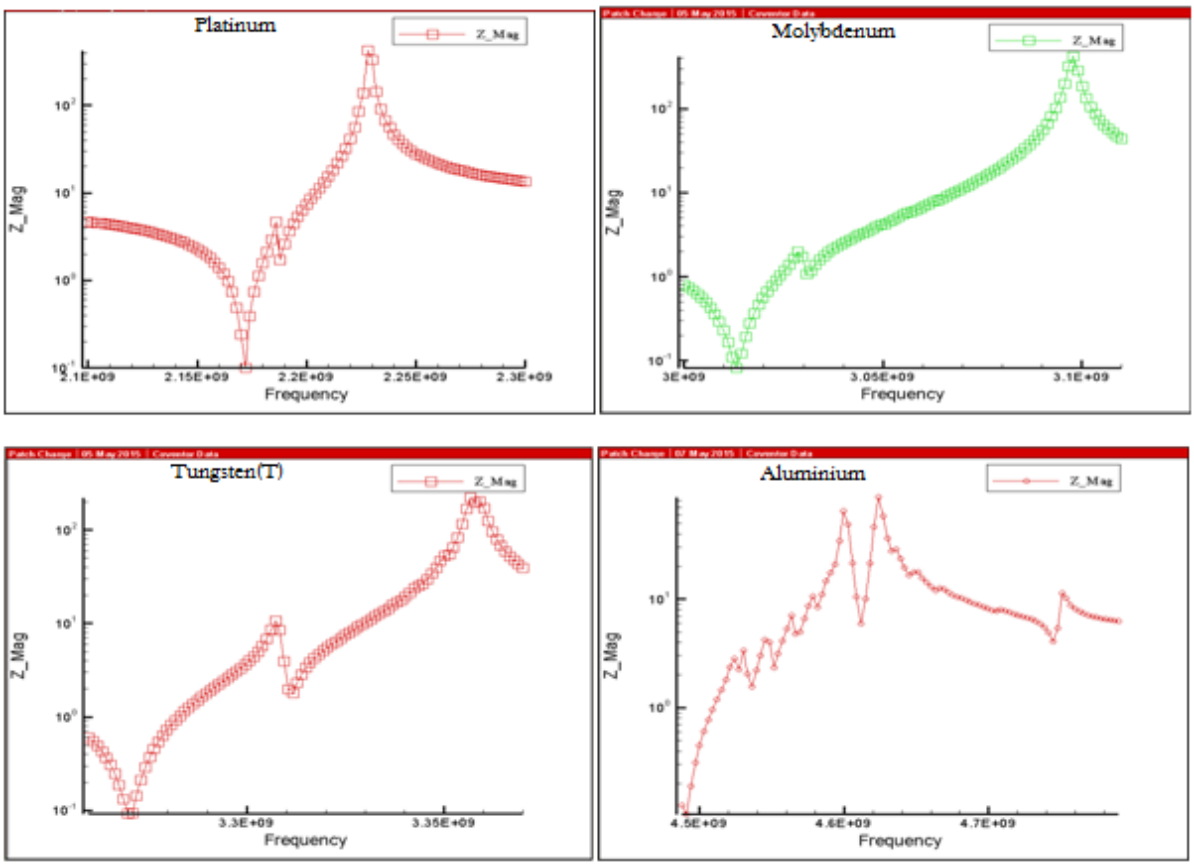

Figure 4-6 Impedance magnitude

Impedance responses of the entire configurations are shown in the figure 4.6.

Chapter 5 Results and discussion

5.1 Effects of different electrodes

5.1.1 Analytical results

The thickness of the device is assumed as the AlN is 1μm. In this analysis, acoustic impedance and acoustic velocities are calculated from the stiffness and density of the material. Coupling coefficient, resonant frequency, anti-resonant frequency, quality factor, bandwidth and FOM are calculated. By using the properties, acoustic velocity and acoustic impedance are calculated by using the following equations

$$v_a = \sqrt{\frac{c}{\rho}} \qquad \text{and} \qquad z = \sqrt{\rho c}$$

Table 5-I Calculated sonic velocity and impedances

Material	Density (g/cm^3)	Stiffness (10^{11}Pa)	Sonic velocity (10^3m/s)	Acoustic impedance ($10^7 kg/m^2s$)
AlN(002)	3.26	3.95	11.007	3.588
ZnO(002)	5.68	2.109	6.093	3.461
SiO_2	2.2	0.7	5.6	1.2
Pt	21.5	3.5	4.034	8.6747
Al	2.7	1.1	6.383	1.723
Mo	10.2	3.92	6.2	6.323
W	19.2	5.2	5.204	10

Coupling coefficients are calculated by using equation

$$K^2 = \frac{e^2}{c^E \varepsilon^S}$$

$$K_t^2 = \frac{e^2}{c^D \varepsilon^S} \qquad \text{where } c^D = c^E(1+K^2)$$

Table 5-II Coupling coefficient

Material	AlN	ZnO
e_{33}	1.55	1.32044
c^E_{33}	3.95	2.109
ε^S_{33}	9.5	10.204
c^D	4.2028	2.28
K^2	0.064	0.08102
K^2_t	0.06017	0.075

Now the table shown below has the resonant frequency, quality factor, effective coupling coefficient etc.

The resonant frequency can be given as

$$\omega_{a,n} = (2n+1)\frac{\pi}{2}\frac{v}{d+t}$$

$$\omega_r = \frac{v_a}{2d}\left(\pi^2 - 8K_t^2\right)^{\frac{1}{2}}$$

Now, when the frequencies are obtained, then the coupling coefficient can be calculated by using the following expression.

$$K_{eff}^2 = \frac{\pi^2}{4}\frac{f_s}{f_p}\left(\frac{f_p - f_s}{f_p}\right)$$

Quality factor can be calculated by using the definition i.e. total energy stored to the losses of the energy per cycle.

$$Q = \frac{v_a^2 \rho}{\omega \eta}$$

As we have both the coupling coefficient and the quality factor, then the FOM can be easily obtained by simply multiplying both the quality factor and coupling coefficient.

$$FOM(f) = k_{eff}^2 * Q(f)$$

Table 5-III AlN sandwiched device parameter with different electrodes

AlN(1µm) Electrode → Parameters ↓	Platinum(Pt)	Aluminium(Al)	Tungsten(w)	Molybdenum(Mo)
F_p(GHz)	3.02627	3.6232	3.367	3.591
F_s(GHz)	2.9466	3.534	3.284	3.502
Bandwidth(MHz)	79.632	89.3	83.22	88.755
K_{eff}^2	6.3%	5.925%	5.94%	5.94%
Q	558	465	501	470
FOM	35.22	27.55	29.8	28

Table 5-IV ZnO sandwiched device parameter with different electrodes

ZnO(1µm) Electrode → Parameters ↓	Platinum(Pt)	Aluminium(Al)	Tungsten(w)	Molybdenum(Mo)
F_p(GHz)	2.098	2.36	2.255	2.353
F_s(GHz)	2.033	2.288	2.185	2.28
Bandwidth(MHz)	64.8	72.97	69.7	72.7
Q	235.8	209.4	219.3	217.8
FOM	17.4	15.5	16.2	16.1

5.1.2 Simulation results

The thickness of the device is assumed as the AlN is 1μm and top and bottom electrode as 0.15 μm thick. This configuration is over a SiO_2 layer and the substrate is silicon, which is fully etched from the back side window. In this simulation, the results collected are resonant and anti resonant frequency, its quality factor and the curve of the impedance and also the capacitance of the device i.e. C_0. From the simulated results, other parameters of the BVD equivalent circuit of FBAR are calculated.

Table 5-V Simulated result of AlN sandwiched device with different electrodes

AlN piezoelectric	Platinum (top and bottom)	Aluminum (top and bottom)	Tungsten (top) Aluminum(bottom)	Molybdenum (top and bottom)	Tungsten (top and bottom)
Fs (GHz)	2.17167	4.4903	3.2705	3.01319	2.34637
Fp (GHz)	2.2314	4.62334	3.3597	3.1024	2.41588
Q	735.5	360	530.5	650	820
Co (pF)	9.4937	9.48057	9.4935	9.48563	9.483068
Cm (pF)	0.53	0.5701	0.525	0.57	0.57
Lm (nH)	10.15	2.206	4.5	4.9	7.78
Rm (ohms)	0.188	0.1728	0.175	0.145	0.1452
Effective coupling	6.42%	5.88%	6.37%	6.88%	6.89%

5.2 Effect of Damping

The performance of the FBAR is influenced by the various geometric parameters and losses from piezoelectric material such as material damping. The quality factor of the FBAR is closely related to the damping. Damping is the dissipation of the energy of the vibrating material. Rayleigh damping is the damping form implemented in FEM simulation tools. It is a linear combination of mass and stiffness matrices. This comes from complex molecular structure interaction with the material. Its estimation is difficult because it changes from sample to sample. This design is simulated for the variation in the damping factors and is found that the quality factor is inversely proportional to the damping, as shown in figure 5.2.

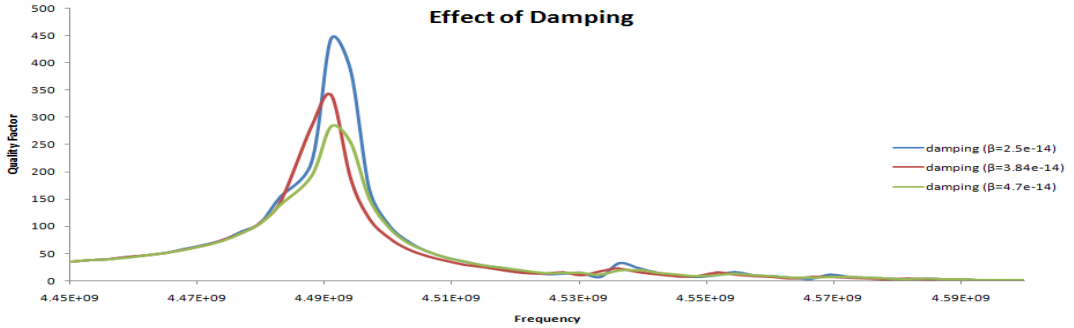

Figure 5-1 Quality factor variation due to damping variation

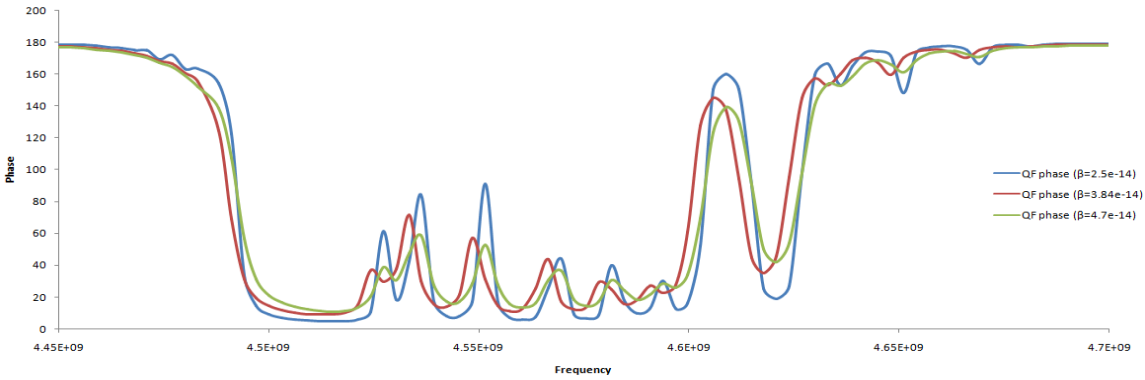

Figure 5-2 Phase variation by damping variation

5.3 Suppressing the spurious modes

There are number of spurious modes in the active reason to remove by different methods.

5.3.1 Apodization

This method is used to change the parallel side of the top electrode to the anti parallel to stop the making of the standing waves in the reason. The 3D model of the simulated structure is shown in figure 5.3.

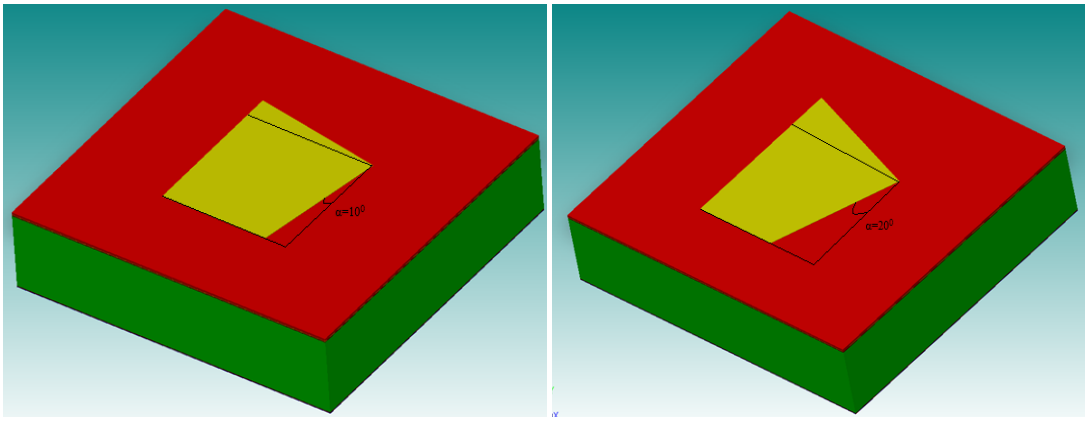

Figure 5-3 Apodization (a) $\alpha=10^0$ and (b) $\alpha=20^0$

Due to Apodization, the losses reduce and the quality factor increases as shown from the following figures.

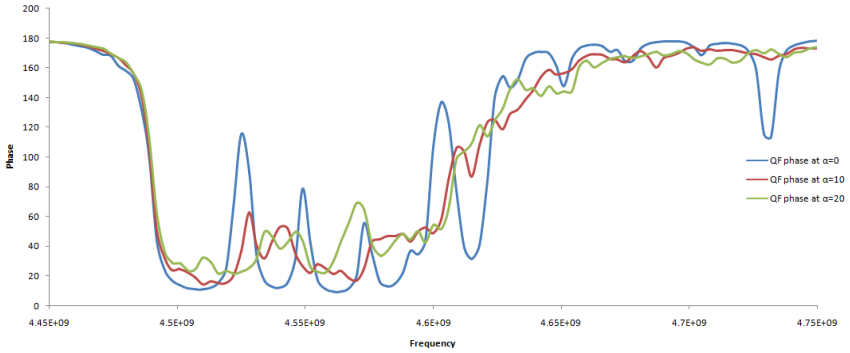

Figure 5-4 Phase variations due to Apodization

5.3.2 Masses at corners

For the simulation of the mass at corners, Comsol Multiphysics software is used. In this simulation, the 2D structure is used for simulation. Two designs are used to suppress the spurious mode. In this mass loading at the corners, the stiffness of the outer boundary are increased due the mass loading and so the lateral waves does not pass through this and all the energy confined in the area. The structure of the simple device and the mass loaded device are shown in the figure 5.5.

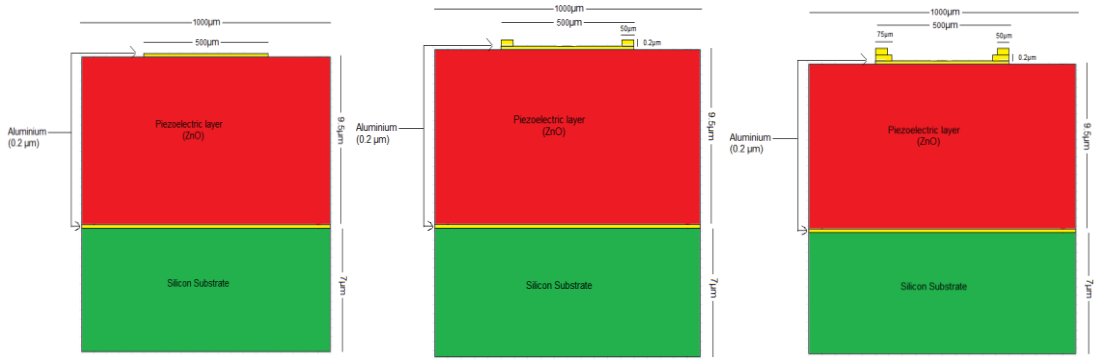

Figure 5-5 Design of the structure of masses at corners (a) normal, (b) 1 step layer, (c) 2 step layer

The sizes of the extra layers are 0.2 µm thickness and side is 50 µm for 1 step size and for 2 steps, the bottom layer is of 75 µm and the upper layer is 50 µm. The response of the FBAR is simulated is as follows

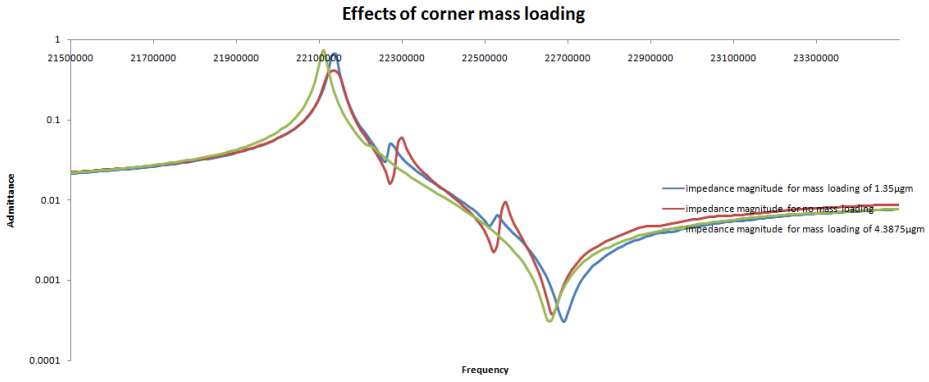

Figure 5-6 Response of admittance for the different step masses on corners of top electrode

5.3.3 Anchor losses

FBAR energy losses are also through the anchor. The anchor of the device is the part on which the FBAR stands and due to no acoustic mismatch, the energy passes through the bottom layer and reduces the quality factor. So in this simulation the area of the anchor is reduced and changes in the quality factor are calculated.

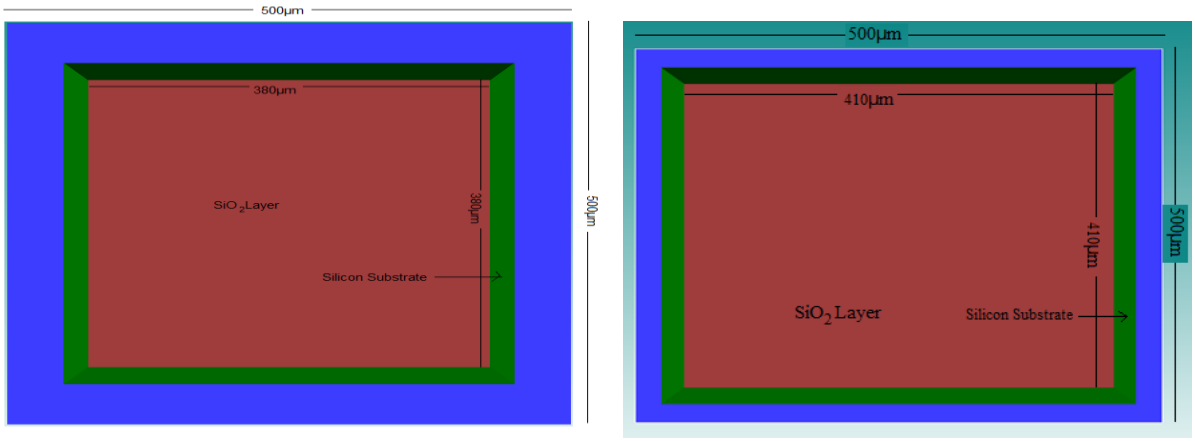

Figure 5-7 Back side of the FBAR (a) 60µm boundary (b) 45µm boundary

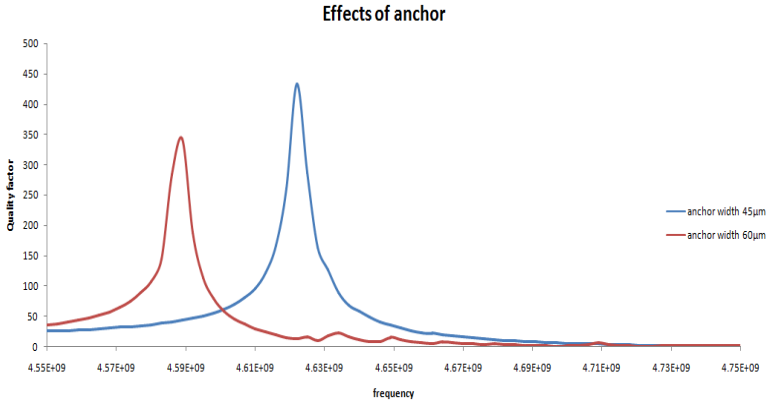

Figure 5-8 Response on the change in anchor area

5.4 FBAR as mass detector application

FBAR can be used as a mass detector application as it changes its resonant frequency as the mass is deposited on the top electrode. This method is used for the detection of the explosive and other materials in the environment by using the adhesive layer on the top electrode that helps in depositing of the mass. The simulations were carried out for the different amount of mass and the changes in resonant frequency were obtained. The design of the mass loaded structure is simulated by using Comsol software and is shown in the following figure.

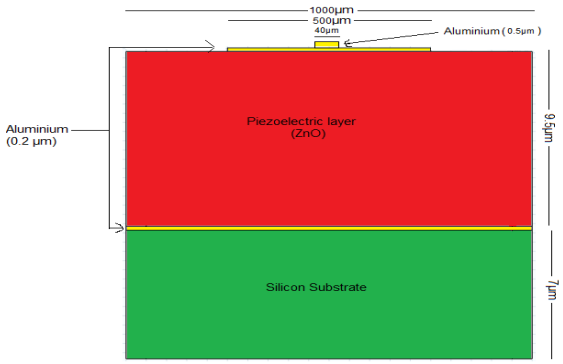

Figure 5-9 Design of mass loading with mass having a thickness of 0.5 µm and side (a) 20 µm, (b) 40µm, (c) 60 µm

The frequency shift of the FBAR due to increase in mass is simulated and shown in the following figure.

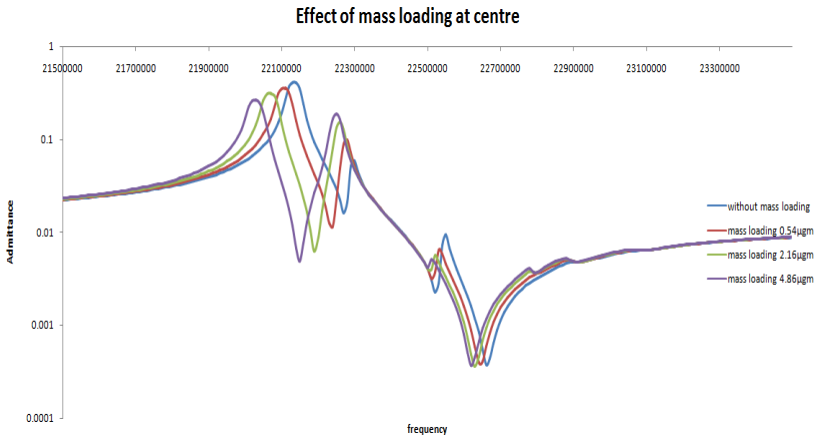

Figure 5-10 Frequency shift by mass loading

The sensitivity of the FBAR is calculated in the terms of frequency per unit of mass. The sensitivity obtained from the following simulation is 205.7 MHz/µ gram.

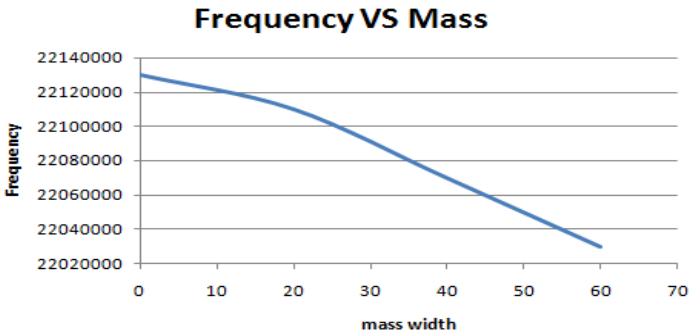

Figure 5-11 Frequency Vs Mass loading

5.4.1 Effect of the position of mass loading

The mass loading over the top of the FBAR is very sensitive to the position of the mass. In the 2D simulation of the FBAR, the position of the mass variance in the positive x direction from the center of the top electrode and the simulation is carried out for the change in the position. The mass taken for

the simulation is the side size of 40 µm and thickness of 0.5 µm with a total mass of 2.16 µgm. The response of this arrangement at the centre is shown in the figure 5.11. The next design and the responses are shown in the following figure.

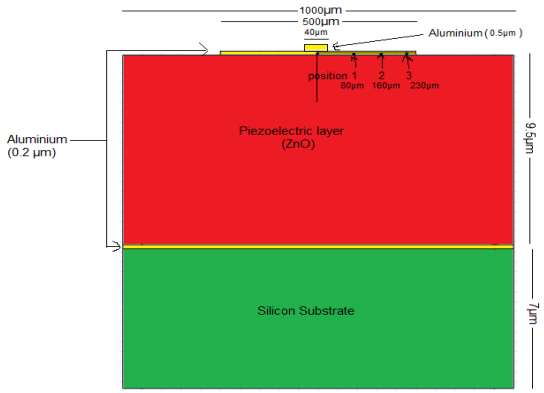

Figure 5-12 Distance of the mass from the center of top electrodes (a) 80µm (b) 160µm, (c) 230µm

The responses of the mass in the term of the admittance are shown in the figure 5.13.

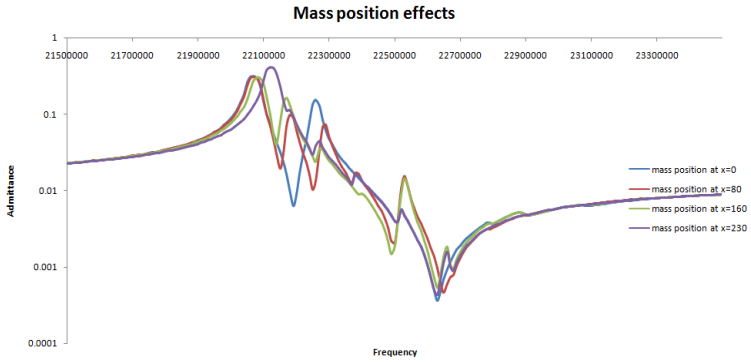

Figure 5-13 Effect of position variation in mass to the admittance

5.5 Effect of change in area of electrode

The top electrode of the FBAR is simulated for the different area to find the variation in the impedance of the device. The effect of increase in area increases the conductivity and so the resistivity decrease. The device is simulated for the top electrode of square structure of side 150 µm, 300 µm and 400 µm. The quality factor and impedances of the device are shown in figure 5.14.

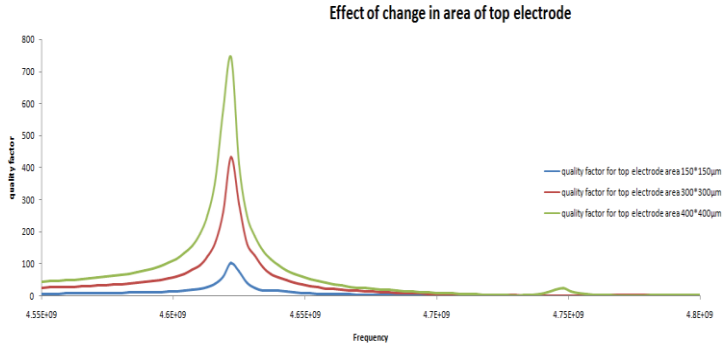

Figure 5-14 Effect of area change on Quality factor

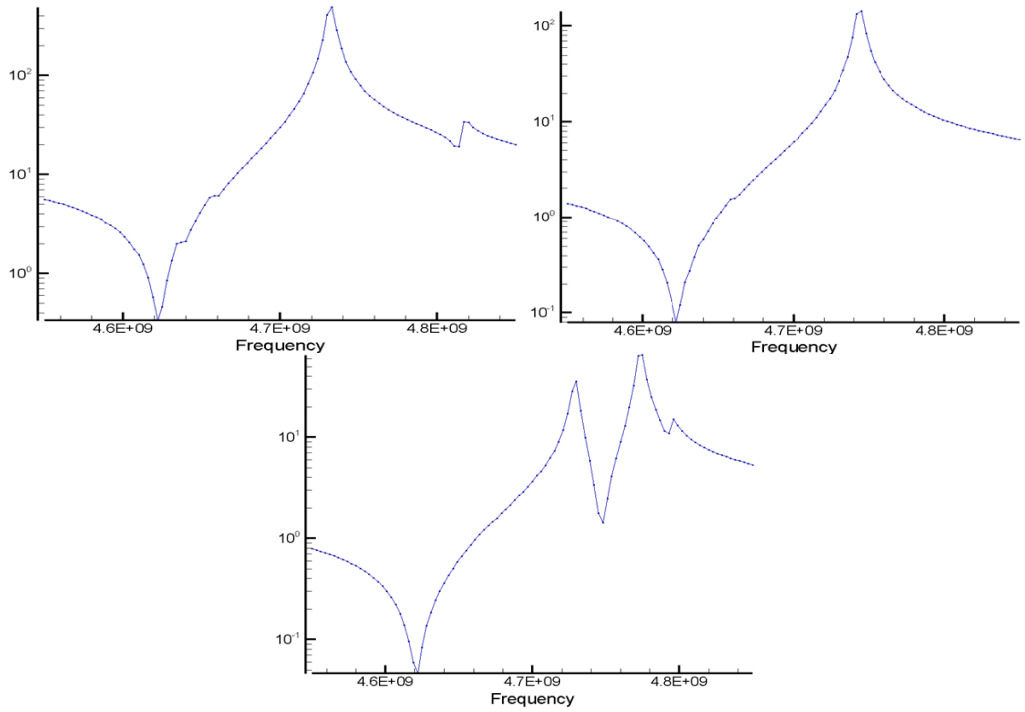

Figure 5-15 impedance response to the change in top electrode (a) 150 µm, (b) 300 µm, and (c) 400 µm

5.6 Discussion

The results from the table 5.3 to 5.5 show that there is a difference between the analytical results and the simulated results, because of the assumption before deriving the expressions, e.g. 1D effect is taken into account only, electrode's less effect *etc*.

1) Now, from AlN simulated and analytical result's table, there is a difference between the resonant frequencies. For the platinum, the resonant frequency is lesser for simulated result, but higher for the aluminium. In the analytical calculation, it is assumed that the electrodes have the same acoustic velocity as the piezolayer but it is not true. For this calculation, the electrode acoustic velocity values are taken into account and average velocity is used to find the resonant frequency. Because the resonator's electrode works as the mirror of the FBAR and try to confine the energy in resonator. For this the acoustic impedance mismatch required between the electrode and air is very large i.e. electrodes must have the high acoustic impedance and so the less acoustic impedance of the air causes the reflection. From table 5.1, the acoustic impedance of the platinum is 8 times of the aluminium. The energy wave travels fully to the platinum and reflects back from the air-electrode junction. Therefore, electrode effects taken into account. In the case of aluminium, the mismatching of acoustic impedance start from the piezoelectric-electrode junction. Some of the energy reflected back from the junction and the rest is from the air-aluminium junction. Lesser the effect of the aluminium in the device and higher the resonant frequency. To take this effect into account, the expression, modified and reflection coefficient is introduced.

$$\omega_{a,n} = (2n+1)\frac{\pi}{2}\frac{v}{d+t}\left(\frac{1}{reflection..coefficient}\right)$$

This reflection coefficient is taken between the piezoelectric layer and electrode layer.

From Table 5.5, the device can be picked up according to the requirement of the resonant frequency, coupling coefficient and quality factor. If the requirement is of very high resonant frequency then the aluminium is the best choice and if the coupling is required very high then platinum is the best. Also, if the requirement is intermediate then molybdenum fulfil the all needs.

2) FBAR is the filter mostly used to filter the signal for the communication purpose like in duplexer. For the maximum transmission of power and less reflection coefficient, the impedance matching is required in the communication channel. The standard impedance adopted is 50 ohms. It is required to make the impedance of the FBAR also equal to standard. In FBAR, one can control the impedance by controlling the area of the electrode. The expression given to the resistance as

$$\hat{R}_a = \frac{4}{\pi}\frac{Z_T}{Z_s}\frac{k_t^2}{\omega_0 C_0}$$

Z_T is the acoustic impedance of piezolayer and Z_s is the acoustic impedance of substrate layer, C_0 is the capacitance. Resistance is inversely proportional to the area of the electrodes.

Let's take an example such that C_0 is 9.49 pF and resonant frequency is 3.27 GHz for an AlN peculiar FBAR. So the impedance will be 7.9 ohms. For the same configuration, let 50 ohms resistance is required and then the area of the capacitor calculated to be around 14000 μm^2. This area can be obtained by number of dimensions.

3) For verification of the effect of the area on the resonant frequency, numbers of simulations are done in the different areas of electrode but there is no change in the resonant frequency. Although there is a very small change detected. The resonant frequency decreases very little as the area of the electrode is increased and this is due to the loading effect of the electrode material. The loading affects the resonant frequency and decrease it, causes the resonant frequency difference in the aluminium and platinum electrode device. Platinum has the highest density and weight. Platinum load the device and causes the decrease in the resonant frequency. While the aluminium is a light material and does not affect the resonant frequency that much.
4) The quality factor of a device indicates the total energy in the device to the losses per cycle. For a good FBAR resonator most of the energy must be confined in the system and the losses should be less. Lower bandwidth is requiring for communication because most of the spectrum is used already. The chances of interference and data losses are higher. To send the information without losses and optimally, a smaller bandwidth is beneficial and high quality factor is required. From the simulated result table 5.5, it is seen that platinum provides a good quality factor and aluminium gives the low quality factor because of high energy losses. Table 5.3 and 5.5 shows the parameters of AlN FBAR but the quality factor of analytical calculation is low because for the simplicity of the calculation, only the strain energy takes into account.
5) Coupling coefficient is also a very important parameter. It is highly dependent on the fabrication of the device like the piezoelectric layer's orientation, which is required to be

in C-axis orientation, roughness of the layers. From the table 5.5, it is clear that platinum and molybdenum have the good coupling coefficient but aluminium is not.

6) The spurious modes in the FBAR can be removed by reducing the damping, use of Apodization and the mass loading at corner. The anchor losses also affect the energy of the FBAR and can be reduced by finding the optimum resonant frequency.

Chapter 6 Layer Deposition and Characterization

In this chapter, the deposition of the Al and AlN layer on the silicon wafer is done. This process of layer deposition is followed by the steps of wafer cleaning, spin coating, photolithography and then the sputtering of the both layers Al and AlN.

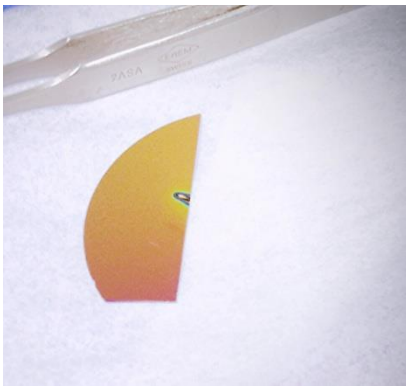

Figure 6-1 AlN layer on Al electrode on Silicon substrate

6.1 Wafer cleaning

The substrate of silicon is used for the deposition of the layers on it. N type silicon wafer is used and the <100> crystal orientation is preferred.

The main objective of wafer cleaning is

- Removal of particle contamination
- Removal of organic contamination
- Removal of metallic/ionic contamination
- Improvement of surface roughness
- Removal of native oxide

The sources of contamination on the wafers may be due to process equipment, ambient gas, chemical, organic vapours in ambient, ash etc.

There are a number of cleaning process used in labs are as follows

- RCA wet cleaning
- Piranha cleaning
- TCE-acetone-methanol cleaning etc.

For our sample, we use the piranha cleaning. In piranha cleaning, the solution of H_2SO_4 and H_2O_2 is mixed in the ratio of 3:1 resp. The sample is washed with DI water. This process may cause the oxidation in the nano scale and so to remove it, the sample is dipped in conc. HF solution. The process of piranha cleaning is given in the appendix.

6.2 Photolithography

It is the process of transferring an image from a photographic mask to a resultant pattern on a wafer. A photosensitive polymer film is applied to the silicon wafer, dried and then exposed with the proper geometric patterns through a photo-mask to UV light or other radiation and finally developed. Depending on the polymer used, either exposed or non exposed area of the film is removed in the developing process.

For the processing of photolithography, requirements are resist, spinner, mask, mask aligner, developer solution, baking ovens etc. Resist is made sensitive to UV light. There are 2 kind of photo resist i.e. positive and negative. Negative photoresist become less soluble in developer solution when they exposed to the radiation where positive photoresist become more soluble after expose.

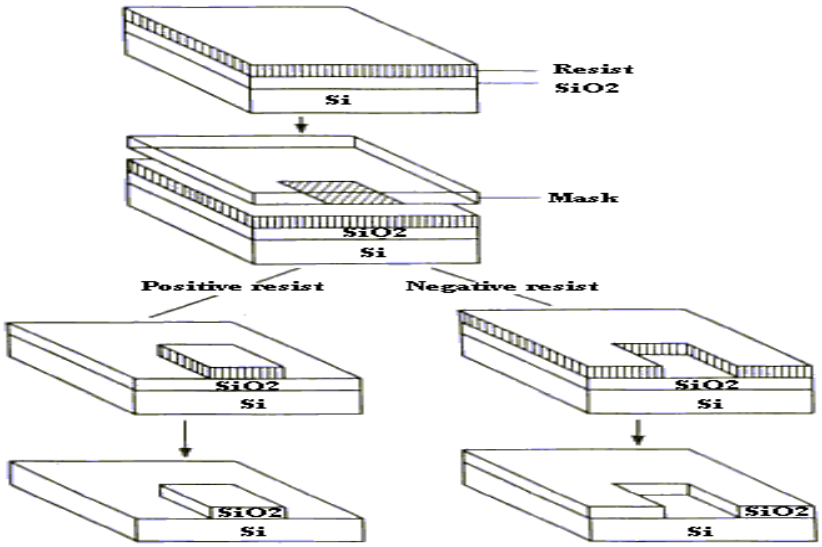

Figure 6-2 Positive and Negative Photolithography

There are no of steps use to transfer the pattern on the wafer. A mask is required for this process first. Mask making is done on the chromium coated glass plate and exposed as per the mask data and then developed to obtain the photo-mask. The mask data is the information contained the geometrical feature corresponding to the particular mask which is electronically entered with the help of a layout editor software e.g. L-edit. The resist of choice i.e. positive or negative is spin coated over the wafer with the spin coater of speed 3000 to 4000 rpm. A layer of adhesion is used between the wafer and resist of Hex-methyl di-silazane (HMDS) to increase the adhesion. Then the coated wafer is put in pre baking process for 30 min. Wafer then exposed to the UV radiation, then dip in the developer solution to expose the pattern. After this the post baking is done. The process used for the sample photolithography is given in the appendix.

6.3 Sputtering

Sputtering deposition is a physical vapour deposition process for depositing thin films.

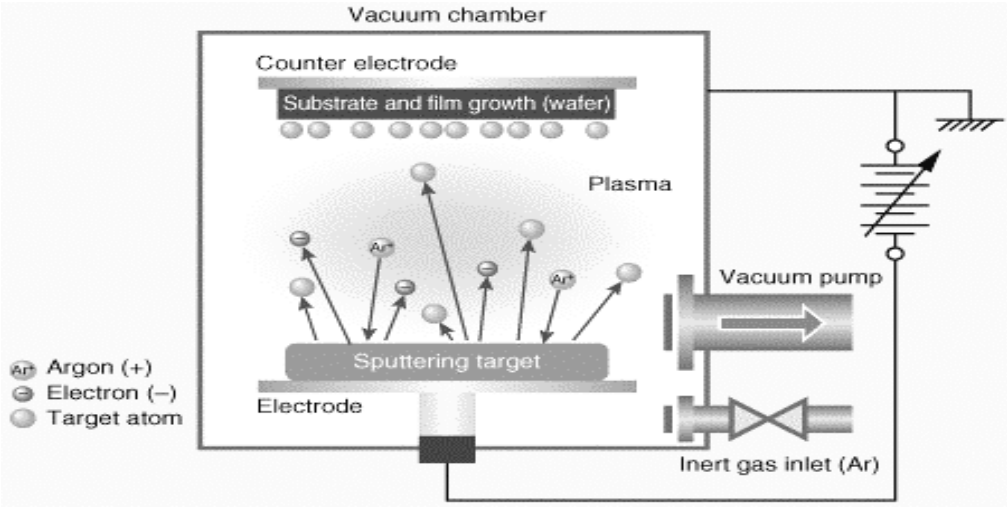

Figure 6-3 Sputtering machine set up

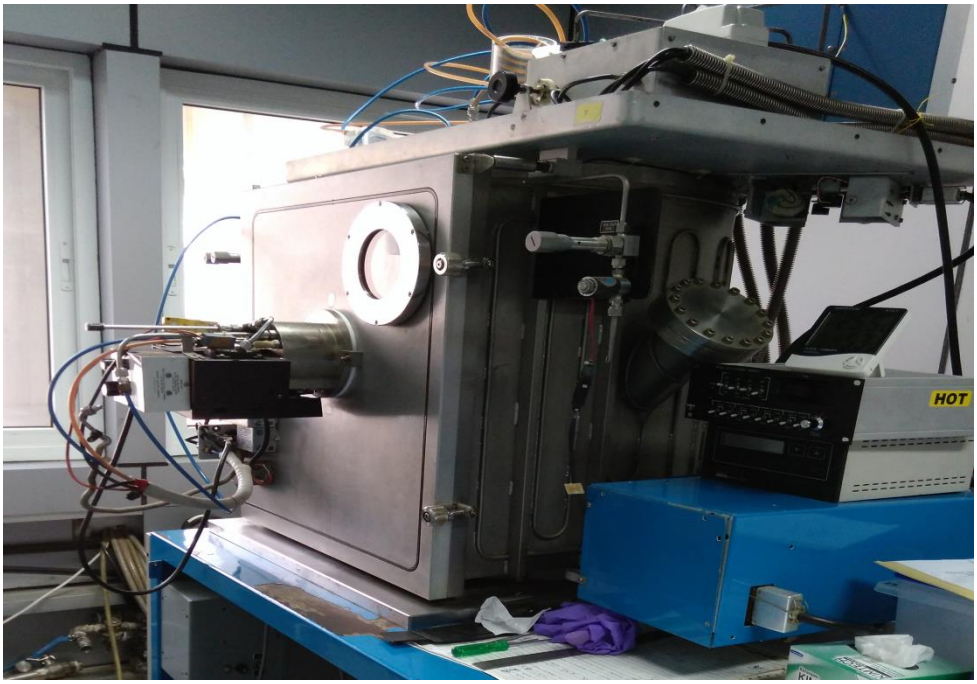

Figure 6-4 Sputtering Machine

Sputtering means ejecting the material from the target and deposited the thin layer on the substrate e.g. silicon wafer. The substrate is put in the vacuumed chamber under the process pressure required. Sputtering will start when the negative voltage is applied to the target and this causes the formation of plasma. This causes the plasma of positive gas ion and then attract towards the negatively charged target. It strikes with a very high speed and cause a momentum transfer. This energy transfer causes the ejection of the atomic size particle and deposited as the thin film over a substrate. The parameter set for the sputtering is given in the appendix.

6.4 Layer characterization

For the layer characterization, some techniques are used, i.e. SEM, EDS, FTIR etc. The results of the following results are shown in the figure below.

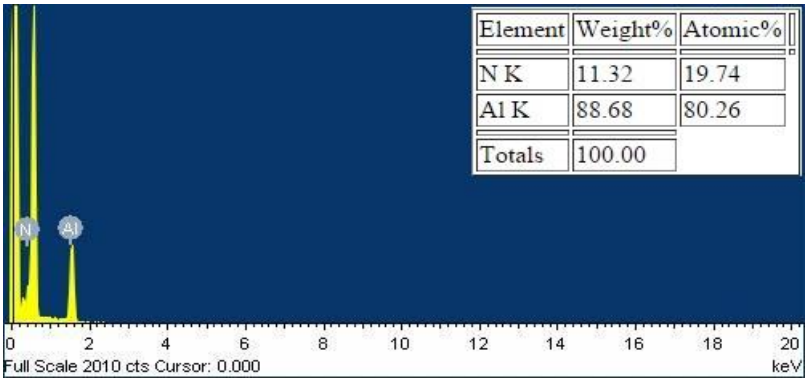

Figure 6-5 EDS graph of AlN

EDS is abbreviated as energy dispersive spectroscopy. FTIR stands for Fourier transform infrared spectroscopy.

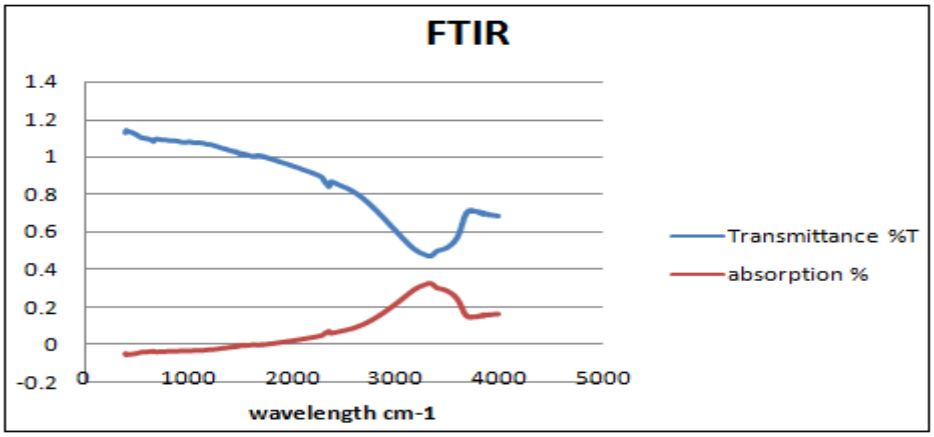

Figure 6-6 FTIR response of AlN sample

Figure 6-7 FTIR set up

Chapter 7 Conclusion and Future Work

7.1 Conclusion

In the present work, a thin film bulk acoustic wave resonator has been designed and simulated for the resonant frequencies, quality factor and impedance characteristics. Analytical study of the resonator is done and results like resonant frequency, coupling coefficient, quality factors are compared with the simulated results. By keeping the same design, electrodes are changed and different parameters are obtained and compare to each other. The platinum and tungsten has found the higher coupling coefficient than aluminium. Aluminium has the higher frequency than the tungsten. The parameters of the equivalent BVD i.e. series and parallel capacitance, inductance and resistance are also calculated. The effect of area change in the top electrode for impedance change has simulated and found that losses decrease as the area increased because of the decrease in impedance. The Apodization technique is simulated for the suppression of spurious modes. The effect of mass loading at centre for frequency shift is simulated and frequency shift is obtained. Suppression of spurious mode by mass loading at the corners and the sensitivity of the different position were simulated. The sensitivity found to be decrease as the mass shifted towards the corner. Effect of damping and the anchor losses were also simulated. The quality factor increases as the damping reduces. Also the losses through the anchor reduces as the area of anchor resuces.

7.2 Future work

- Characterization of the AlN film over the different electrode like Al, Pt, Mo, W etc
- Piezoelectric response of the AlN layer
- Fabrication of the device and characterization

References

1. K.M. Lakin and J.S. Wang, "Acoustic bulk wave composite resonators", *Applied physics let.* 38(1981) 125-127
2. W. Mueller, "a brief overview of FBAR technology", Agilent Technology (technical report), July 20,2001
3. R. Ruby, P. Bradley, J Larson III, Y. Oshmyanski and D. Figueredo, "Ultra-Miniature High Q filter and Duplexer using FBAR technology", in *IEEE Intl. Solid State Circuit Conf. Dig. of Tech. Papers*, Feb 5-7 2001,San Francisco, CA, USA, 120-121
4. K.M. Lakin, J.R. Belsick, J.P. McDonald, K.T. McCarron and C.W. Andrus, "Bulk Acoustic Wave Resonator and Filter for Application above 2 GHz", in *IEEE International Microwave symp. MTT-S 2002 Digest of Tech. Papers*, Jun 3-7 2002, Seattle, WA, USA, 3, 1487-1490
5. M. Ylilammi, J. Ella, M. Partanen and J. Kaitila, "Thin Film Bulk Acoustic Wave Filter", *IEEE T. Ulatrason. Ferroelec. Freq. Control 49*,4(2002) 535-539
6. C.S. Lu, "Application of Piezoelectric quartz crystal Microbalance", Elsevier, London, 1984
7. H. Zhang, M.S. Marma, E.S. Kim, C.E. McKenna and M.E. Thompson, "A Film Bulk Acoustic Resonator in Liquid Environments", J. *Micromech. Microeng.* 15(2005) 1911-1916
8. H. Zang, J. Kim, W. Pang, H. Yu and S. Kim, "5 GHz low phase noise oscillator based FBAR with low TCF", *in Proc. 13th International Conference on Solid-State Sensor, Actuator and Microsystems Transducers 2005*, Jun 5-9 2005, Seoul, Korea, 1100-1101
9. Weigel, R., et al., "Microwave Acoustic Material, device, and Application", *IEEE Trans. MTT, Vol 50, No.3*, March 2002, pp 738-749
10. K.M. Lakin, K.T. McCarron, and J.F. McDonald, "Temperature Compensated Bulk Acoustic Thin Film Resonators", *Proceeding of IEEE Ultrasonic Symp. 2000, San Juan, Puerto Rico*. 855-858
11. M. Ueda, et al., "High Q Resonator using FBAR/SAW Technology and Their Application", *Proceeding of IEEE IMS-MTT-S 2005*, Long Beach, CA, 2005
12. R. Brederlow, et al., "Biochemical Sensor Based on Bulk Acoustic Resonator", Electron Device Meeting, 2003, Technical Digest, Dec 8-10, 2003, pp. 32.7.1-32.7.3
13. J.D. Larson, et al., "Modified Butterworth-Van Dyke circuit for FBAR Resonator and automated measurement system", *proceeding of IEEE Ultrasonic Symp.* 2000, San Juan, Puerto Rico, pp. 863-868
14. S.H. Chang, N.N. Rogacheva, and C.C. Chou, "Analysis of Method for Determining Electromechanical Coupling coefficient of Piezoelectric Element", *IEEE Trans. On Ultrasonic, Ferroelectric and Frequency Control*, Vol. 42, No. 4, July 1995, pp. 525-541

15. E.L. Adler, “Matrix Method Applied to Acoustic Waves in Multilayer”, *IEEE Trans. On Ultrasonic, Ferroelectric and Frequency Control*, Vol. 37, No. 6, Nov 1990, pp. 485-490
16. R. Thalhammer, et al., “Spurious Modes Suppression in BAW Resonator”, *Proceeding of IEEE Ultrasonic Symp. 2006*, Vancouver, Canada, pp. 456-459
17. J.D. Larson and Y. Oshmyansky, “Measurement of effective kt2, Q, Rp, Rs, Vs Temperature for Mo/AlN FBAR Resonator”, *Proc. 2002 IEEE Ultrasonic Symp.*, pp. 939-943
18. K.M. Lakin, et al., “Temperature Coefficient and Ageing of BAW Composite Material”, *Proc. Frequency Control Symp. 2001*, pp. 605-608
19. K.M. Lakin and K.G. Lakin, “Numerical Analysis of Thin Film BAW Resonator”, *IEEE Int. Ultrasonic Symp. 2003*, pp. 4A-3
20. J. Bjurstrom, et al., “Dependence of Electromechanical Coupling on the Degree of Orientation of C-textured Thin AlN Films”, *IEEE Trans. On Ultrasonic, Ferroelectric and Frequency Control*, Vol. 51, 2004, pp. 1347
21. I. L. Guy, E. M. Goldys, and S. Muensit, “Measurements of Piezoelectric Coefficients of Nitride Semiconductor Films”, Semiconducting and Insulating Materials Conference, 2000. SIMC-XI. International, July 3-7 2000, pp. 55-58
22. R. Ruby, R. Parker, and D. Feld,”Method of Extracting Q Applied Across Different Resonator Technologies”, *Ultrasonics Symp.*, 2008
23. M. C. Chao, Z. N. Huang, S. Y. Pao, Z. Wang, and C.S. Lam, “Modified BVD-equivalent circuit of FBAR by taking electrodes into account”, in Proc. *IEEE Intl. Ultrason. Symp. 2002*, Oct. 8-12-2002, Munich, Germany, 973-976
24. D.Rosen, J. Bjursttrom, and I. Katardjiev, “Suppression of Spurious lateral modes in Thickness-excited FBAR resonators”, *IEEE T. Ultrason. Ferroelectr. Freq. Control* 52(2005) 1189-1192
25. W. Pan, P. Soussan, B.Nauwelaers, and H.A.C. Tilmans, “A surface micromachined electrostatically tunable film bulk acoustic resonator”, *Sens. Actuator A-Phys.* 126(2006) 436-446
26. F. Vanhelmont, P. Philippe, A.B.M. Jansman, R.F. Milsom, J.J.M. Ruigrok, and A. Oruk, “A 2 GHz Reference Oscillator incorporating a Temperature Compensated BAW Resonator”, in *Proc. IEEE Intl. Ulrason.Symp.,* 2006, Oct. 3-6 2006, Vancouver, Canada, 333-336
27. R. Ruby, “Review and Comparison of Bulk Acoustic Wave FBAR and SMR Technology”, IEEE Proceeding Int. Ultrasonic symp. 2007, paper 11E-3
28. P. Muralt, “Is there a better Material for Thin Film BAW Application than AlN”, *IEEE Proceeding Int. Ultrasonic symp. 2005*, paper 5C1
29. H.P. Loebl, et al., “Piezoelectric Material for BAW Resonator and Filter”, *IEEE Proceeding Int. Ultrasonic symp. 2001*, paper 807-811
30. K. Tsubouchi, K. Sugai, and N. Mikoshiba, "AlN Material Constants Evaluation and SAW Properties on AlN/Al2O3 and AlN/Si," *IEEE Ultrasonics Symposium Proceedings*, pp. 375-380, 1981

31. J.B. Lee, J.P. Jung, M.H. Lee and J.S. Park, “Effect of Bottom Electrode on the Orientation of AlN films and the Frequency response of resonator in AlN based FBARs”, *Thin Solid Films* 447-448, 2004
32. Q. Su, P. Kirby, E. Komuro, M. Imura, Q Zhang and R. Whatmore, “Thin Film Bulk Acoustic Resonator and Filter using ZnO and lead-zirconium-titanium thin films”, *IEEE T. Microwave Theory Tech. 2001*, pp. 769-778
33. E. Forsen, G. Abadal, S. Ghatnekar-Nilsson, J. Teva, J. Verd, R. Sandberg, W. Svandsen, et al., “Ultrasensitive mass sensor fully integrated with complimentary MOS circuitry”, Applied Physics Letter 2005, 043507-1-3
34. Nurul I. M. Nor, et al., “Estimation of Material Damping Coefficient of AlN for FBAR”, ICFMM 2014, Malaysia
35. Krishnaswamy, S.V et al., “Film Bulk Acoustic Resonator Technology”, Ultrasonics Symposium, 1990
36. Yoon, Giwan; Jae-Don Park; Park, Hee-Dae, “Characterization of ZnO-Based FBAR Devices for RF Applications” Microwave and Millimeter Wave Technology, 2000, 2nd International Conference on. ICMMT 2000
37. Qingming Chen *et al*., “Materials Property Dependence of the Effective Electromechanical Coupling Coefficient of Thin Film Bulk Acoustic Resonators” 2004 IEEE International Ultrasonics, Ferroelectrics and Frequency Control Joint 50th Anniversary Conference
38. Lakin, K.M.et al., “Wide Bandwidth Thin Film BAW Filters”, 2004 IEEE International Ultrasonics, Ferroelectrics and Frequency Control Joint 50th Anniversary Conference
39. Wei Pang et al., “Self-Aligned Lateral Field Excitation Film Acoustic Resonator with Very Large Electromechanical Coupling” 2004 IEEE International Ultrasonics, Ferroelectrics and Frequency Control Joint 50th Anniversary Conference
40. Mathios Link et al., “Solidly Mounted ZnO Shear Mode Film Bulk Acoustic Resonators for Sensing Applicationsin Liquids” ieee transactions on ultrasonics, ferroelectrics, and frequency control, vol. 53, no. 2, february 2006
41. Linh Mai et al., “Design and Fabrication of ZnO-Based FBAR Microwave Devices for Mobile WiMAX Applications” IEEE microwave and wireless components letters, vol. 17, no. 12, december 2007
42. Wei Pang et al., “Electrical Frequency Tuning of Film Bulk Acoustic Resonator” Journal of microelectromechanical systems, vol. 16, no. 6, december 2007
43. Xu Zhang et al., “Thermal Analysis and Characterization of a High Q Film Bulk Acoustic Resonator (FBAR) as Biosensers in Liquids” Micro Electro Mechanical Systems, 2009. MEMS 2009. IEEE 22nd International Conference
44. J. Oiler et al., “THE SENSITIVITY ENHANCEMENT FOR THE RADIATION SENSOR BASED ON FILM BULK ACOUSTIC-WAVE RESONATOR” Solid-State Sensors, Actuators and Microsystems Conference (TRANSDUCERS), 2011 16th International
45. Gancede L.G. et al., “ZnO-Based FBAR Resonators With Carbon Nanotube Electrodes” Ultrasonics, Ferroelectrics, and Frequency Control, IEEE Transactions, 2011

46. Kochhar A. Et al., "Monolithic Fabrication of Film Bulk Acoustic Resonators above Integrated Circuit by Adhesive- Bonding-Based Film Transfer" Ultrasonics Symposium (IUS), 2012 IEEE International

Appendix A Fabrication parameters

A.I Cleaning process

Step-1 Wafer dip in piranha solution for 10 minutes (150 ml H_2SO_4 + 50 ml H_2O_2)
Step-2 Wash with DI water
Step-3 HF dip for 7 minutes (170ml DI + 30ml HF), use Teflon glass
Step-4 Wash with DI water and dip in it
Step-5 Dry wafer by nitrogen gun
Step-6 Baking the wafer in oven at 180^0C
Step-7 Clean the beakers

A.II Photolithography

Step-1 Put wafer on the chuck of spin coater properly in the environment of temperature of 20^0C, humidity 66% and yellow light environment
Step-2 Rotate chuck at the speed of 3400rpm for 30 sec
Step-3 Put the HMDS solution to increase the adhesion and rotate for 90 sec
Step-4 Put S-1818 photoresist on the wafer and rotate for 30 sec
Step-5 Take sample out and clean chuck
Step-6 Put the wafer in oven for prebaking at 90^0C for 25 minutes
Step-7 Now expose the sample to the UV light under the mask
Step-8 Dip in the developer MF-319 for 40 sec to expose the pattern
Step-9 Rinse with DI water
Step-10 Dry with Nitrogen
Step-11 Hard baking at the 120^0C for 30 sec

A.III Sputtering

Table 7-I Sputtering parameters for the AlN and Al

Parameters	AlN	Al
Power	250W	250W
Sputtering voltage	500V	532V
Rotation of chuck	50 RPM	50 RPM
Plasma slab time	2 min	4 min
Ar/N_2 conc.	50/50%	100/0%
CP before sputtering	3.5e-5 torr	2.6e-5 torr
Cp during sputtering	5.6e-3 torr	5e-3 torr
Sputtering rate	8nm/min	20nm/min

PUBLICATIONS

1. Kumar Y., Agarwal R., Kamaljit R., "Design and Simulation of Film Bulk Acoustic Resonator (FBAR) with different electrode configurations" *Journal of Microelectromechanical System, (communicated)*
2. Kumar Y., Agarwal R., Kamaljit R., "Design and Simulation of Film Bulk Acoustic Resonator (FBAR) for Quality Factor Enhancement" *Journal of Microelectromechanical System, (communicated)*

Yatin

ORIGINALITY REPORT

5%	3%	2%	3%
SIMILARITY INDEX	INTERNET SOURCES	PUBLICATIONS	STUDENT PAPERS

PRIMARY SOURCES

1	Submitted to Thapar University, Patiala Student Paper	1%
2	www.readbag.com Internet Source	<1%
3	Submitted to Indian Institute of Technology, Bombay Student Paper	<1%
4	Nor, N.I.M., N. Khalid, Rozana A.M. Osman, and Z. Sauli. "Estimation of Material Damping Coefficients of AlN for Film Bulk Acoustic Wave Resonator", Materials Science Forum, 2015. Publication	<1%
5	www.leatherheadfood.com Internet Source	<1%
6	www.ags.uci.edu Internet Source	<1%
7	www.coventor.com Internet Source	<1%
8	dspace.thapar.edu:8080 Internet Source	<1%